

Can a particle's motion distinguish scale-dependent Planck stars from renormalization group improved Schwarzschild black holes?

Li Huang^{1,2} and Xue-Mei Deng^{1,*}

¹*Purple Mountain Observatory, Chinese Academy of Sciences, Nanjing 210023, China*

²*School of Astronomy and Space Science, University of Science and Technology of China, Hefei 230026, China*



(Received 6 February 2024; accepted 8 May 2024; published 3 June 2024)

We investigate the differences between a test timelike particle's motions around scale-dependent Planck stars and its motions around renormalization group improved Schwarzschild black holes in detail. By introducing the positive or negative sign of the parameter s (with $s = -1$ and $s = +1$ denoting scale-dependent Planck stars and renormalization group improved Schwarzschild black holes, respectively), we present the circular orbital characteristics of both scale-dependent Planck stars and renormalization group improved Schwarzschild black holes. This shows the existence of stable and unstable circular orbits and the dependence of the innermost stable circular orbit on a dimensionless parameter $|\tilde{\omega}|(\gamma, \lambda_{\mp})$, where $|\tilde{\omega}|$ comes from the theory of nonperturbative renormalization groups, γ is the identification of the cutoff for the distance scale, and λ_{\mp} are two new dimensionless normalized parameters. In comparison to the black holes, the parameter γ has more influence on stable and unstable circular orbits for the scale-dependent Planck stars. Specifically, we calculate the particle's relativistic periastron advance for the two models and give a preliminary bound on scale-dependent Planck stars and the renormalization group improved Schwarzschild black holes by using the result of the S2 star's precession with observations from GRAVITY. The bound we obtain in the present work is $s|\tilde{\omega}| = (-0.80 \pm 1.53) \times 10^{92}$. By using the shadow result from EHT, the bound on $s|\tilde{\omega}|$ is improved by up to 3 or 4 orders of magnitude, which is $-1.36 \times 10^{88} \lesssim s|\tilde{\omega}| \lesssim 2.32 \times 10^{89}$. It suggests that a primordial black hole or even a mini-black hole can give a tighter bound on two spacetimes in the future. While we need to break the parameters' degeneracy for the two models with future observations, the negative value in our bound suggests that the existence of Planck stars may be possible. We also intensively compare the particle's periodic orbits around Planck stars with those around the black holes. It is found that small variations in λ_{\mp} make the particle's orbits alternate back and forth from periodic to quasiperiodic orbits, or even jump to nonbound orbits in two spacetimes. We discuss briefly the gravitational waveforms generated from the periodic motions for a small body which orbits a supermassive Planck star or a supermassive black hole, which exhibit some distinct phases and amplitudes for the two models. Our results show that it might be possible to aid in the identification between two spacetimes by using the particle's motion.

DOI: [10.1103/PhysRevD.109.124005](https://doi.org/10.1103/PhysRevD.109.124005)

I. INTRODUCTION

After more than a century, Einstein's general relativity is an extraordinarily successful theory of gravity and has passed a wealth of tests from our Solar System to binary pulsar systems and exoplanets [1–4]. These great successes, however, have never stopped alternatives from being proposed due to some problems in classical general relativity, such as the singularity and the event horizon of the Schwarzschild black hole. Especially, thanks to technical advancements that have resulted in the detection of gravitational waves from binary black hole mergers [5–10], in images of the supermassive black holes in the centers of M87 and our Galaxy [11–22], and in the detection of Schwarzschild precession in

the orbit of the star S2 around Sgr A* [23], probing general relativity and new physics beyond the current paradigm in the strong gravitational field have recently opened a new era in astronomy and gravitational theory [24–68].

Inspired by a well-accepted and self-consistent quantum gravity theory, scale-dependent gravity is of great interest, and these modified metrics are thought to automatically incorporate the effects of quantum gravity. As for the subclass scale-dependent gravity, renormalization group improved Schwarzschild black holes [69,70] and scale-dependent Planck stars [71] have been proposed by introducing a “running” Newton's constant G through the relationship between the arbitrary renormalization energy scale k and the radial coordinate r . One benefit from the “running” constant is the removal of the central singularity and its replacement with one (anti-)de Sitter

*xmd@pmo.ac.cn

core by some quantum influences. The parameter $\tilde{\omega}$, which comes from nonperturbative renormalization group theory, appears in the “running” constant. Although the value of theoretical prediction for $\tilde{\omega}$ is not unique [72–77] the semi-classical Newtonian potential, the number is nearly order 1 by comparing the semi-classical Newtonian potential with an effective theory (see Table 1 in Ref. [78] for more details, but with a different symbol). When $\tilde{\omega}$ is positive, the scale-dependent gravity turns to the renormalization group improved Schwarzschild black hole scenario [69,70] and keeps the gravity “asymptotically safe” from divergences. Some interesting properties for these black holes have been well investigated in strong deflection lensing [45], in thermodynamics [69], in the quantum gravitational effects on accretion [79], in cosmological perturbations [80], and in the dynamics of test particles around the black holes [81].

By contrast, if one relaxes the sign of $\tilde{\omega}$ and allows the parameter to be negative, it leads to a specific metric called scale-dependent Planck stars [71]. This new metric is able to describe some important characteristics for Planck stars without further assumptions (see Ref. [71] for details). For instance, the stars can be identical with classical Schwarzschild black holes at a large radial coordinate and match with the Donoghue quantum-corrected potential [72,73,75,76]. The size of the anti-de Sitter core turns out to be exactly that of the Planck stars [82] in a quite natural way. Furthermore, its Hawking temperature, specific heat, emission rate equation, and thermodynamic entropy have been considered intensively in Ref. [71], whereas bound orbits around scale-dependent Planck stars and a comparison between a test timelike particle’s motions around Planck stars and its motions around renormalization group improved Schwarzschild black holes are still missing in the literature.

A timelike particle’s bound orbits around black holes are a useful tool for understanding gravitation and some remarkable properties of black holes. As the most simple bound orbits, circular orbits play an important role in astrophysics and contribute to modeling a rotating/charged black hole and constraining the parameters of the spin and the charge. A lot of previous research focuses on circular geodesics and their dynamical characteristics (see [83–105] and references therein). Circular orbits around scale-dependent Planck stars and black holes will be examined in this paper. It is worth noting that the circular orbits of massive/massless particles have been fully considered in regular black holes [106] recently. It has been found that the characteristics of these circular orbits are classified into four cases depending on the strength of the charge. The corresponding method in Ref. [106] will be adopted in the present work.

As one subclass of bound orbits, the precessing ones—more specifically, the periastron advances of our Solar System’s planets [107–113], of binary pulsars [114–119], and of exoplanets [4,120–122]—are paving the way for

probing the general relativity and modified gravity scenarios in the weak gravitational field. Particularly, with GRAVITY’s observation [23], the precession of the S2 star around Sgr A* lays the foundation for testing alternatives and new physics in the gravitational field of a supermassive black hole. It motivates us to test the scale-dependent Planck stars and the renormalization group improved Schwarzschild black holes and distinguish the Planck stars from the black holes in the Galactic Center using the precessing orbit of the S2 star.

When a timelike particle locates in the vicinity of one black hole, on the other hand, its bound orbits exhibit the zoom-whirl behaviors [123–126], which correspond to periodic orbits and belong to the strong gravitational field feature. This feature is described by the ratio of the average angular frequency to the radial frequency per radial cycle [127]. Periodic orbits can offer computational advantages for an extreme-mass-ratio inspiral system [128] and are devoted to studying the gravitational radiation in the system [129–131]. Besides this, the zoom-whirl behaviors may be observed in the future and will provide unique insights into some properties of the spacetime in the strong gravitational field. Given this, the periodic orbits have been examined in the vicinities of classical black holes [127,132], of some modified black holes [131,133–155], and of binary black holes [156,157]. Recently, it has been suggested that the set of all periodic orbits could be charted in the energies and angular momenta plane [158].

Triggered by the above observational and theoretical progresses, and for the sake of distinguishing the scale-dependent Planck stars from the renormalization group improved Schwarzschild black holes by the timelike particle’s motions—namely, $\tilde{\omega}$ —we will mainly explore the circular, precessing, and periodic orbits around two spacetimes in the present paper, providing some information about their signatures in the timelike particle’s motions. However, these approaches in the present work are phenomenological. In the quantum system, there are three general constants, which are the Planck length l_p , the Planck mass m_p , and the Planck time. These are very small quantities. Considering that strong gravity effects are only just being studied by existing experiments, such as the GRAVITY and Event Horizon Telescope (EHT) observations, it is possible that quantum corrections to general relativity can arise at these large scales. We want to start with some rough estimates first for these quantum-corrected effects at such large scales.

We define one deviation quantity $\eta \equiv (\mathbb{O}_{\text{Quan}} - \mathbb{O}_{\text{Schw}}) / \mathbb{O}_{\text{Schw}}$, where \mathbb{O}_{Schw} and \mathbb{O}_{Quan} represent the observables for the Schwarzschild black hole and the quantum-corrected one, respectively (e.g., scale-dependent Planck stars or the renormalization group improved Schwarzschild black holes). For scale-dependent and mass-dependent experiments, we hypothesize

$$\eta \sim \tilde{\omega} \left(\frac{l_p}{L} \right) \left(\frac{m_p}{m_*} \right) \quad (1)$$

in the steady system at the leading term. In Eq. (1), $\tilde{\omega}$ is the dimensionless parameter we mention above and can be regarded as the strength of coupling between gravity and the quantum system. m_* is the mass of the central body in one experimental system and L is the experimental system scale. Due to the steady system, the Planck time does not appear in Eq. (1). For the present high-precision experiments, the central bodies that have been observed are almost supermassive black holes, which leads to $m_p/m_* \simeq 10^{-45}$. For the other ratio l_p/L , it yields to 10^{-49} for GRAVITY's observation and to 10^{-46} for EHT's observation. It makes the value of $\tilde{\omega}$ very large in these large scales if the quantity $\eta \sim 1$. Even now, there exist some observations for stellar-mass black holes ($10m_\odot$), and for the experimental system scale located on their event horizons, we still obtain $m_p/m_* \simeq 10^{-39}$ and $l_p/r \simeq 10^{-40}$. It also suggests that, detecting such a modification, the quantum corrections would have to come about at scales much larger than the Planck length. However, such an experiment has not yet been done.

The paper is organized as follows: In the next section, we concentrate on the timelike particle's circular orbital characteristics for scale-dependent Planck stars and renormalization group improved Schwarzschild black holes. Section III describes the particle's relativistic periastron advance and the shadow size for two spacetimes, and it estimates a preliminary bound using the data detected by GRAVITY and EHT. Section IV exhibits the particle's periodic motions and the corresponding gravitational waveforms around the Planck stars and black holes in the strong gravitational field. Finally, Sec. V presents conclusions and prospects for future work.

II. METRIC, GEODESICS, AND CIRCULAR ORBITS

The metric for the scale-dependent Planck stars [71] and the renormalization group improved Schwarzschild black holes [69,70] with m_* reads

$$ds^2 = -A(r)dt^2 + B(r)dr^2 + C(r)d\Omega^2, \quad (2)$$

where $d\Omega^2 = d\theta^2 + \sin^2\theta d\phi^2$ and (t, r, θ, ϕ) are the Schwarzschild coordinates with a $(-, +, +, +)$ metric signature. In metric (2), we have

$$A(r) = [B(r)]^{-1} = 1 - \frac{2Gm_*}{c^2 r} \left(1 + s|\tilde{\omega}| \frac{G\hbar}{c^3 r^2} + \gamma s|\tilde{\omega}| \frac{G^2 \hbar m_*}{c^5 r^3} \right)^{-1}, \quad (3)$$

$$C(r) = r^2, \quad (4)$$

in which the dimensionless parameter γ is positive and comes from an identification of the cutoff of the corresponding distance scale [69,70]. Another dimensionless parameter $\tilde{\omega}$ belongs to the nonperturbative renormalization group theory and could be positive or negative [69–71]. We introduce the sign “ s ” in front of $|\tilde{\omega}|$ in Eq. (3) for convenience. Therefore, $s = -1$ and $s = 1$ denote the scale-dependent Planck stars and the renormalization group improved Schwarzschild black holes, respectively. When γ and $\tilde{\omega}$ become zero, the metric (2) is exactly the same as the prediction by the general relativity. In the present work, we adopt $G = c = \hbar = 1$ and $\Omega = |\tilde{\omega}|/m_*^2 \geq 0$. The lapse (3) yields

$$A(r) = [B(r)]^{-1} = 1 - \frac{2m_*}{r} \left(1 + s\Omega \frac{m_*^2}{r^2} + \gamma s\Omega \frac{m_*^3}{r^3} \right)^{-1}. \quad (5)$$

Note that G , c , and \hbar can be returned to Eq. (5) at all times according to dimension analysis. For instance, $m_* \rightarrow Gm_*/c^2$ and $s|\omega| = s\Omega(Gm_*^2)/(\hbar c)$ in SI units. And $s|\omega| < 0$ represents the scale-dependent Planck stars [71], while $s|\omega| > 0$ denotes the renormalization group improved Schwarzschild black holes [69,70].

For the scale-dependent Planck stars and the renormalization group improved Schwarzschild black holes, the existence of the event horizon(s) has been investigated in Refs. [69–71] through the lapse function $A(r)$. There exists only one event horizon for the scale-dependent Planck stars, while the renormalization group improved Schwarzschild black holes may have one, two, or no event horizon(s). $A(r) = 0$ gives the following cubic equation [45]:

$$r^3 - 2m_* r^2 + s\Omega m_*^2 r + \gamma s\Omega m_*^3 = 0, \quad (6)$$

and the discriminant of the above formula [45] is

$$\Delta_3 = -m_*^6 \Omega s (\Omega - s\Omega_+) (\Omega - s\Omega_-), \quad (7)$$

with

$$\Omega_\pm = -\frac{27}{8}\gamma^2 - \frac{9}{2}\gamma + \frac{1}{2} \pm \frac{1}{8} \sqrt{(\gamma+2)(9\gamma+2)^3}. \quad (8)$$

We then obtain that $\Omega_+ > 0$ and $\Omega_- < 0$ because of $\gamma > 0$.

For the scale-dependent Planck stars ($s = -1$), Eq. (7) becomes $\Delta_3 = m_*^6 \Omega (\Omega + \Omega_+) (\Omega + \Omega_-)$. We have $\Omega + \Omega_- \geq 0$ in order to ensure $\Delta_3 \geq 0$. Thus, a dimensionless parameter λ_- can be defined as follows:

$$\lambda_- \equiv \frac{\Omega}{\Omega_-} \leq 0. \quad (9)$$

It means that Eq. (7) for $s = -1$ has one or two roots when $-1 \leq \lambda_- \leq 0$ (e.g., $\Delta_3 \geq 0$) and no roots for $\lambda_- < -1$

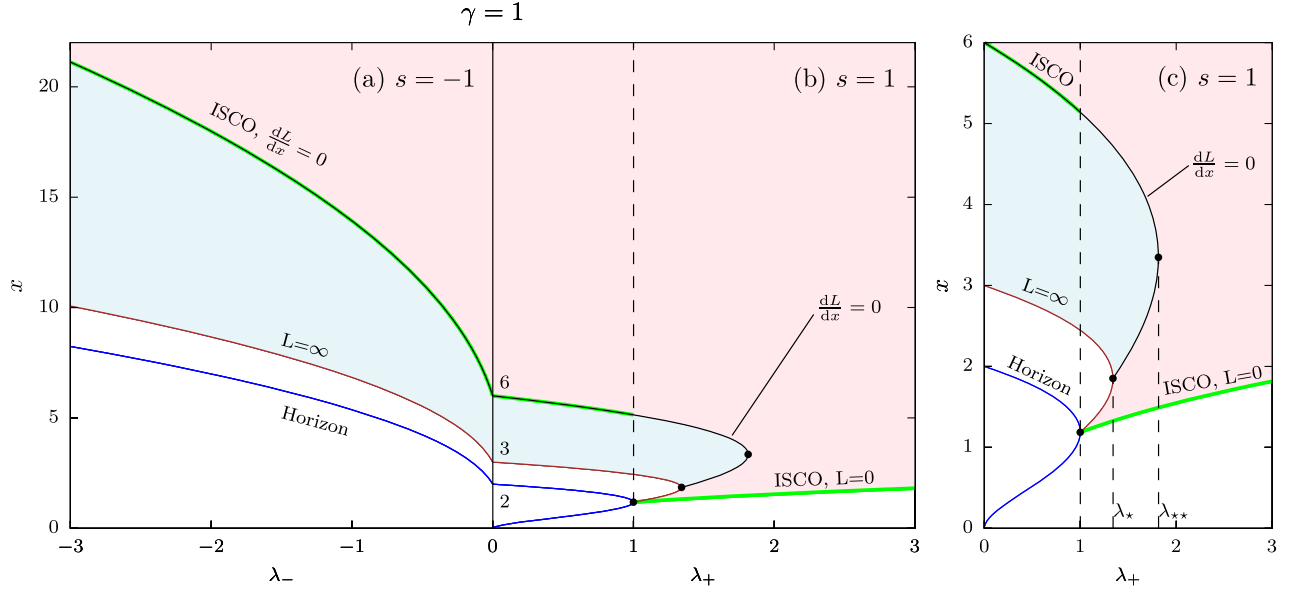


FIG. 1. Existence of circular orbits for a timelike particle with (a) scale-dependent Planck stars ($s = -1$) and (b) renormalization group improved Schwarzschild black holes ($s = 1$), plotted in (λ_{\mp}, x) -space for $\gamma = 1$. (c) Zoomed-in view of (b). A particle located in the light red region has stable circular orbits, and a particle located in the light blue region belongs to unstable circular orbits. In the white regions, however, there exist no circular orbits. Blue solid lines depict the event horizon(s). The red solid lines correspond to lightlike orbits based on Ref. [106], and the lines only for the model $s = 1$ split into two branches at λ_* (see the closeup in the right panel). The green and black solid lines represent the innermost stable circular orbit (ISCO), and the lines only for $s = 1$ split into two branches at λ_{**} (see the closeup in the right panel).

(e.g., $\Delta_3 < 0$). Clearly, the event horizon(s) only locates in the physical region for $r > 0$. It is not difficult to find that there exists only one event horizon for the case of $s = -1$ graphically (see the blue solid line in the left figure of Fig. 1), which is consistent with the result in Ref. [71]. For a large distance scale, namely $m_* \rightarrow \infty$, the behavior of the event horizon for the scale-dependent Planck stars is $2Gm_*/c^2 + (2 + \gamma)|\tilde{\omega}|\hbar/(4cm_*)$. For a small distance scale, however, the event horizon becomes $\sqrt{|\tilde{\omega}|G\hbar/c^3} + (1 + \gamma/2)Gm_*/c^2$ (see Ref. [71] for details). Here, we switch the dimension back.

The similar theoretical analysis has been done for the renormalization group improved Schwarzschild black holes ($s = 1$) according to the cubic equation (7) [45]. By introducing the dimensionless parameter

$$\lambda_+ \equiv \frac{\Omega}{\Omega_+} \geq 0, \quad (10)$$

it is found that Eq. (7) has one or two positive roots when $0 \leq \lambda_+ \leq 1$ in order to ensure $\Delta_3 \geq 0$. And there are no roots for the condition of $\lambda_+ > 1$ (see Refs. [45,69] for details). These roots are all located in the physical region for $r > 0$, which corresponds to the event horizon(s) in renormalization group improved Schwarzschild black holes. The behavior of the event horizon has been shown in the right panel of Fig. 1 with the blue solid line.

In summary, when $s = -1$, there is always one event horizon with $\lambda_- < 0$. When $s = 1$, the existence of the event horizon(s) depends on the value of λ_+ . There are two event horizons with $\lambda_+ \in (0, 1)$: when $\lambda_+ = 1$, two event horizons merger into one; and when $\lambda_+ > 1$, there is no event horizon. See the blue solid lines in Fig. 1. It should be noted that the scale-dependent Planck stars and the renormalization group improved Schwarzschild black holes reduce to Schwarzschild black holes when $\lambda_- = \lambda_+ = 0$. With the introduction of two dimensionless parameters λ_- and λ_+ , we can see that the scale-dependent Planck stars depend on λ_- and γ [e.g., $\Omega(\gamma, \lambda_-)$ or $|\tilde{\omega}|(\gamma, \lambda_-)$], and the renormalization group improved Schwarzschild black holes depend on $\Omega(\gamma, \lambda_+)$ or $|\tilde{\omega}|(\gamma, \lambda_+)$. In the present work, in order to distinguish the scale-dependent Planck stars from the renormalization group improved Schwarzschild black holes by the timelike particle's motions, we mainly study the influences of the parameters $\Omega(\gamma, \lambda_{\mp})$ on the corresponding circular orbits, on the advances of the periastron in the weak gravitational field, and on the periodic orbits and their gravitational waveforms in the strong gravitational field. We suppose that these will provide some helpful information and insights.

The Lagrangian for a test particle governed by the metric (2) in the equatorial plane ($\theta = \pi/2$) is derived as follows:

$$2\mathcal{L} = -A(r)\dot{t}^2 + B(r)\dot{r}^2 + C(r)\dot{\phi}^2 = \kappa, \quad (11)$$

with $\kappa = 0$ and -1 for a lightlike or a timelike particle, respectively. An overdot denotes the derivative with respect to an affine parameter—e.g., λ . Here, we are not imposing on $A(x)B(x) = 1$ temporarily just for the sake of giving a more general expression. Along the path of the test particle, we obtain two conserved quantities

$$P_t = \frac{\partial \mathcal{L}}{\partial \dot{t}} = -A(r)\dot{t} \equiv -E, \quad (12)$$

$$P_\phi = \frac{\partial \mathcal{L}}{\partial \dot{\phi}} = C(r)\dot{\phi} \equiv L, \quad (13)$$

where E and L indicate, respectively, the conserved energy and the orbital angular momentum of the particle. Substituting Eqs. (12) and (13) into Eq. (11), we have

$$\dot{x}^2 = \frac{E^2}{B(r)A(r)} - \frac{1}{B(r)} \left[-\kappa + \frac{L^2}{C(r)} \right]. \quad (14)$$

For convenience, we define the following dimensionless quantities:

$$x \equiv r/m_*, \quad l = L/m_*. \quad (15)$$

Then, Eq. (14) is reexpressed as

$$\dot{x}^2 = \frac{E^2}{B(x)A(x)} - \frac{1}{B(x)} \left[-\kappa + \frac{l^2}{C(x)} \right] \equiv R(x). \quad (16)$$

For the timelike particle, $\kappa = -1$, we obtain one-dimensional motion for $R(x)$ from Eq. (16). The metric coefficients (3) can be simplified as

$$A(x) = [B(x)]^{-1} \\ = 1 - \frac{2}{x} (1 + s\Omega x^{-2} + \gamma s\Omega x^{-3})^{-1}, \quad (17)$$

$$C(x) = x^2, \quad (18)$$

with $s = -1$ for the scale-dependent Planck stars and $s = 1$ for the renormalization group improved Schwarzschild black holes.

Considering that circular orbits condition and a more general expression for Eq. (16), the timelike particle should satisfy

$$R(x) = 0, \quad (19)$$

$$R(x)_{,x} = 0, \quad (20)$$

where the above expressions reduce to the formula for circular orbits with $A(x)B(x) = 1$ [159,160]. The orbital angular momentum and the energy are derived by functions of the circular orbit radius x_c ,

$$l^2(x_c) = \frac{A'(x_c)C^2(x_c)}{A(x_c)C'(x_c) - A'(x_c)C(x_c)}, \quad (21)$$

$$E^2(x_c) = \frac{A^2(x_c)C'(x_c)}{A(x_c)C'(x_c) - A'(x_c)C(x_c)}, \quad (22)$$

where a prime denotes the derivative with respect to x . It is worth noting that the above more general expressions are independent of the metric coefficient $B(x)$.

As Ref. [106] points out, the physical circular orbits for the timelike particle must satisfy the conditions of $l^2 \geq 0$ and $E^2 \geq 0$. Therefore, the signature of dl/dx_c is opposite to that of $R_{,xx}[x_c, l(x_c)]$ due to

$$R(x)_{,xx} = -R(x)_{,xl} \frac{dl}{dx_c}, \quad (23)$$

$$-R(x)_{,xl} = -\frac{2lC'(x)}{B(x)C(x)[C(x) + l^2]} < 0, \quad (24)$$

where we use $E^2/A(x) = 1 + l^2/C(x)$ based on Eq. (19). The above conditions are identical with those of Ref. [106], where the relationship between the effective potential U in Ref. [106] and $R(x)$ is $R(x) = E - U$, with $A(x)B(x) = 1$. This means that the stable circular orbit can be described by $R(x)_{,xx} < 0$ or $dl/dx_c > 0$. It can be further derived that

$$\frac{dE^2}{dx_c} = \frac{dl}{dx_c} \frac{2lA(x)}{C(x)}, \quad (25)$$

which indicates that dE^2/dx_c has the opposite signature to $R(x)_{,xx}$.

The innermost stable circular orbit (ISCO) describes the minimum radial distance of a test timelike particle around one black hole. When the particle lies in the innermost stable circular orbit [161], its motion cannot enter the event horizon and maintain a stable circular orbit, which satisfies the following conditions:

$$R(x) = 0, \quad R(x)_{,x} = 0, \quad R(x)_{,xx} = 0 \quad (26)$$

for the case of the existence of the event horizon(s). From the above discussion, this suggests that the condition of $R(x)_{,xx} = 0$ is equivalent to that of $dl/dx_c = 0$. This means that, in order to describe the innermost stable circular orbit for the existence of the event horizon(s), $dl/dx_c = 0$ can replace $R(x)_{,xx} = 0$ in Eq. (26). Besides this, by using $A(x)B(x) = 1$ and $R(x) = E^2 - U$, Eq. (26) returns to the result in Ref. [106].

For horizonless black holes, only the renormalization group improved Schwarzschild black holes ($s = 1$) have this situation when $\lambda_+ > 1$; the corresponding innermost stable circular orbit is found as [106]

$$R(x) = 0, \quad R(x)_{,x} = 0, \quad l = 0. \quad (27)$$

This indicates that the innermost stable circular orbit for the horizonless case is described by such specific orbits with zero angular momentum. Furthermore, it is derived that the innermost stable circular orbit radius for $l = 0$ can be obtained from $R(x)_{,x} = 0$.

For the lightlike particle, $\kappa = 0$. Equation (16) then becomes

$$\dot{x}^2 = \frac{E^2}{B(x)A(x)} - \frac{l^2}{B(x)C(x)} \equiv R(x). \quad (28)$$

From Ref. [106], the circular orbits for the lightlike particle read

$$R(x) = 0, \quad R(x)_{,x} = 0, \quad l = \infty. \quad (29)$$

Then, it is found that the radius of the circular orbit for the lightlike particle is obtained from $A(x)_{,x}C(x) - A(x)C(x)_{,x} = 0$. It gives the radius of the sphere, which will be considered in Sec. III B. This result also reduces to the one in Ref. [106] by using $A(x)B(x) = 1$.

To compare the difference between circular orbits around scale-dependent Planck stars and those around renormalization group improved Schwarzschild black holes, the metric coefficients (17) and (18) are now substituted into the above general analysis expressions. Then, we plot Fig. 1, which displays the existence and stability of the circular orbits in the scale-dependent Planck stars ($s = -1$) and the renormalization group improved Schwarzschild black holes ($s = 1$) for $\gamma = 1$. The blue, red, green, and black solid lines depict the event horizon, the circular orbit of the lightlike particle, the innermost stable circular orbit of the timelike particle with the existence of the event horizon(s), and the innermost stable circular orbit of the timelike particle with no horizon, respectively. It suggests that the red and black solid lines are all split into two branches at λ_* and λ_{**} separately only for the case of $s = 1$ (see the closeup in the right panel of Fig. 1 for details). For the case of $s = -1$, however, the situation is quite different, and the three solid lines are all monotonically decreasing. This demonstrates that there exist different behaviors of circular orbits for timelike and lightlike particles between scale-dependent Planck stars and renormalization group improved Schwarzschild black holes. Further analysis reveals that the particles located in the light red regions have stable circular orbits, while the particles located in the light blue regions belong to unstable circular orbits. The regions colored by white show where there exist no circular orbits.

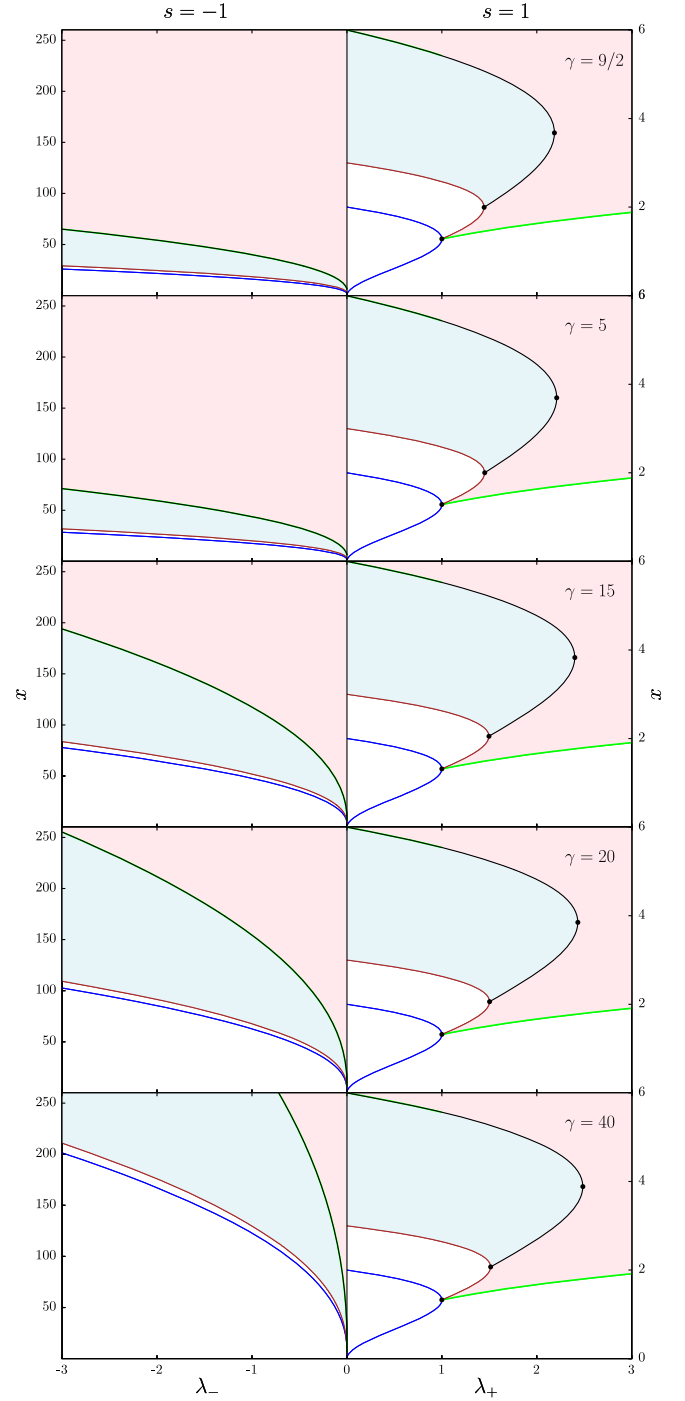


FIG. 2. Existence of circular orbits for a timelike particle with scale-dependent Planck stars ($s = -1$) and with renormalization group improved Schwarzschild black holes ($s = 1$), plotted in (λ_+, x) -space for $\gamma = 9/2, 5, 15, 20, 40$. The meanings of different regions and solid lines in this figure correspond to those of Fig. 1. Note that two vertical coordinates have different scales in two columns in order to study the effect of γ on two spacetimes ($s = -1$ and $s = 1$).

Figure 1 indicates that the scale-dependent Planck stars and the renormalization group improved Schwarzschild black holes will be identical with the Schwarzschild black holes when $\lambda_- = \lambda_+ = 0$. Meanwhile, the *radius* of the event horizon, the circular orbit of lightlike particles and the innermost stable circular orbit for timelike particles for two models ($s = -1$ and $s = 1$) reduce to the corresponding values of the Schwarzschild case, which are $2Gm_*/c^2$, $3Gm_*/c^2$, and $6Gm_*/c^2$, respectively (see Fig. 1). We switch the dimension back here. It is worth mentioning that other situations are almost qualitatively the same when the parameter γ goes to different values. However, we still plot Fig. 2 just to show the influence of γ on the existence and stability of circular orbits in two models ($s = -1$ and $s = 1$) for different values (9/2, 5, 15, 20, 40). From Fig. 2, it can be seen that, as to the renormalization group improved Schwarzschild black holes, the various values of γ have little effect on the regions for stable circular orbits, for unstable circular orbits, and for no circular orbits. Conversely, for the scale-dependent Planck stars, the regions for the circular orbits and for no circular orbits decrease with the increase of γ , but the region for unstable circular orbits increases with the increase of γ . This suggests that there are different effects of the parameter γ on the existence and stability of circular orbits for two spacetimes. These results might provide hints for distinguishing the scale-dependent Planck stars from the renormalization group improved Schwarzschild black holes by the timelike particle's bound orbits.

III. PRELIMINARY BOUND ON THE STRENGTH OF COUPLING PARAMETER

A. Periastron advance

As one kind of bound orbits, periastron advance points the way to the confirmation of Einstein's general relativity [1] and testing competitive modified gravity scenarios [107–113]. In this subsection, we will derive the relativistic periastron advance for timelike particles around scale-dependent Planck stars and renormalization group improved Schwarzschild black holes. A preliminary bound on the scale-dependent Planck stars and the renormalization group improved Schwarzschild black holes will be first given by using the result of the GRAVITY observations for the S2 star [23].

For the timelike particle, the bound orbits can be written by a rational or an irrational number q [127] as

$$\Delta\phi = 2\pi(q + 1). \quad (30)$$

In Eq. (30), q can describe periodic or precessing orbits. During a radial period, the accumulated azimuth $\Delta\phi$ between successive periastron or apastron can be described as

$$\Delta\phi = 2 \int_{r_{\text{pe}}}^{r_{\text{ap}}} \frac{\dot{\phi}}{\dot{r}} dr = 2 \int_{r_{\text{pe}}}^{r_{\text{ap}}} \frac{d\phi}{dr} dr = 2 \int_0^\pi \frac{d\phi}{d\chi} d\chi, \quad (31)$$

where r_{pe} and r_{ap} are the periastron and apastron, respectively, of the bound orbits. When q is an irrational number, the bound orbits display precession (namely, periastron advance) [127].

The radial coordinate can be parametrized as [160]

$$r = \frac{a(1 - e^2)}{1 + e \cos \chi}, \quad (32)$$

with a , e , and χ being the semimajor axis, the eccentricity, and the relativistic true anomaly. The periastron r_{pe} and apastron r_{ap} can be obtained by $\chi = 0$ and $\chi = \pi$ as follows:

$$r_{\text{pe}} = a(1 - e), \quad r_{\text{ap}} = a(1 + e). \quad (33)$$

From Eqs. (13), (14), and (32), we derive

$$\begin{aligned} \frac{d\phi}{d\chi} &= ae(1 - e^2)L \left\{ \frac{E^2}{B(r)A(r)} - \frac{1}{B(r)} \left[1 + \frac{L^2}{C(r)} \right] \right\}^{-1/2} \\ &\times [C(r)]^{-1} (1 + e \cos \chi)^{-2} \sin \chi. \end{aligned} \quad (34)$$

With the fact that the radial velocity \dot{r}^2 at r_{pe} and r_{ap} is zero, E^2 and L^2 are determined by Eq. (14) as

$$E^2 = \frac{A(r_{\text{ap}})A(r_{\text{pe}})[C(r_{\text{ap}}) - C(r_{\text{pe}})]}{C(r_{\text{ap}})A(r_{\text{pe}}) - C(r_{\text{pe}})A(r_{\text{ap}})}, \quad (35)$$

$$L^2 = \frac{C(r_{\text{ap}})C(r_{\text{pe}})[A(r_{\text{ap}}) - A(r_{\text{pe}})]}{C(r_{\text{ap}})A(r_{\text{pe}}) - C(r_{\text{pe}})A(r_{\text{ap}})}. \quad (36)$$

Substituting Eqs. (35) and (36) into Eq. (34), we expand Eq. (34) as the term m_* . One analytic approximation for Eq. (34) is found as

$$\begin{aligned} \frac{d\phi}{d\chi} &= 1 + \frac{e \cos \chi + 3}{a(1 - e^2)} m_* \\ &+ \frac{1}{2} \frac{[e \cos \chi + 3][3e \cos \chi - 2s\Omega + 9]}{a^2(1 - e^2)^2} m_*^2 \\ &+ \mathcal{O}(m_*^3). \end{aligned} \quad (37)$$

The periastron advance of the timelike particle around the scale-dependent Planck stars and the renormalization group improved Schwarzschild black holes can be derived as

$$\begin{aligned}\Delta\omega_{\text{SDPSs/RGIBHs}} &\equiv \Delta\phi - 2\pi \\ &\simeq \frac{6\pi m_{\bullet}}{a(1-e^2)} + \frac{3\pi(18+e^2)m_{\bullet}^2}{2a^2(1-e^2)^2} \\ &\quad - \frac{6\pi s\Omega m_{\bullet}^2}{a^2(1-e^2)^2} + \mathcal{O}(m_{\bullet}^3).\end{aligned}\quad (38)$$

In the above formula, the first and second terms are the first post-Newtonian (1PN) and the second post-Newtonian (2PN) periastron advances of the Schwarzschild black hole in spherical Schwarzschild coordinates [162,163], which are

$$\Delta\omega_{\text{GR}} = \frac{6\pi m_{\bullet}}{a(1-e^2)} + \frac{3\pi(18+e^2)m_{\bullet}^2}{2a^2(1-e^2)^2} + \mathcal{O}(m_{\bullet}^3).\quad (39)$$

The third term in Eq. (38) is the effect of the scale-dependent Planck stars and the renormalization group improved Schwarzschild black holes on the periastron advance. In order to compare two spacetimes by measuring the periastron advance of the S2 star orbiting Sgr A* and to give the preliminary bound on the spacetimes, we keep the terms at the 2PN order (m_{\bullet}^2), because the third term in Eq. (38) appears in the 2PN order.

By means of the four-VLT-telescope interferometric beam combiner instrument, GRAVITY reported the first result of the periastron advance in the orbit of the S2 star orbiting Sgr A* under the Schwarzschild black hole model with the combination of astrometric and spectroscopic measurements of the star [23]. The ratio f_{sp} of the measured periastron advance $\Delta\omega$ to the value $\Delta\omega_{\text{GR}}$ predicted by the Schwarzschild black hole [23] is

$$f_{\text{sp}} \equiv \frac{\Delta\omega}{\Delta\omega_{\text{GR}}} = 1.10 \pm 0.19.\quad (40)$$

Supposing that Sgr A* fits the model of scale-dependent Planck stars or the renormalization group improved Schwarzschild black holes, the periastron advance of the star orbiting the supermassive black hole at the Galactic Center can be modeled by Eq. (38), so that we have the following expression:

$$\begin{aligned}f_{\text{sp}} &\equiv \frac{\Delta\omega_{\text{SDPSs/RGIBHs}}}{\Delta\omega_{\text{GR}}} \\ &\simeq 1 - \frac{s\Omega m_{\bullet}}{a(1-e^2)} + \mathcal{O}(s\Omega m_{\bullet}^2, m_{\bullet}^3),\end{aligned}\quad (41)$$

where we only keep the leading term of $s\Omega$ and neglect the terms of $s\Omega m_{\bullet}^2$ and m_{\bullet}^3 . We can see that f_{sp} in scale-dependent Planck stars and renormalization group improved Schwarzschild black holes only depends on $s\Omega$ or $s|\tilde{\omega}|$. The other parameter, γ , is not sensitive to f_{sp} at the leading term. Therefore, when G , c , and \hbar are

returned to Eq. (41), we deduce the following dimensionless parameters:

$$\begin{aligned}s\Omega &\simeq (1-f_{\text{sp}}) \left(\frac{a}{R_{\text{Schw}}} \right) 2(1-e^2) \\ &= (-0.53 \pm 1.01) \times 10^3\end{aligned}\quad (42)$$

or

$$\begin{aligned}s|\tilde{\omega}| &\simeq (1-f_{\text{sp}}) \left(\frac{a}{l_{\text{p}}} \right) \left(\frac{m_{\bullet}}{m_{\text{p}}} \right) (1-e^2) \\ &= (-0.80 \pm 1.53) \times 10^{92},\end{aligned}\quad (43)$$

where R_{Schw} is the Schwarzschild radius. From Eq. (43), it is shown that we obtain the same relationship between the Planck length/mass and the scale/mass in the experimental system shown in Eq. (1).

In the theoretical point of view, under a quantum-corrected Newtonian potential, $s|\tilde{\omega}|$ can be determined by comparing the semiclassical Newtonian potential $[A(r) - 1]/2$. The value of this theoretical prediction is not unique and is nearly order 1 in various literature. For example, $s|\tilde{\omega}| = 127/(30\pi^2)$ in [72,73], $s|\tilde{\omega}| = 122/(15\pi)$ in [74], $s|\tilde{\omega}| = -41/(10\pi)$ in [75,76], and $s|\tilde{\omega}| = -167/(30\pi)$ in [77]; see Table 1 in Ref. [78] for more details, but with a different symbol. In the practical point of view, high-precision data for black holes come from supermassive black holes at present, such as the GRAVITY observation [23]. Because the experimental system scale $a \simeq 12264R_{\text{Schw}}$ is much larger than the Planck length, and the mass of Sgr A* is also much larger than the Planck mass, this makes the bound on $s|\tilde{\omega}|$ many orders of magnitude larger. In Eq. (43), it is noted that tighter constraints on $s|\tilde{\omega}|$ should be given on a smaller experimental system scale with a smaller central compact body.

In Eqs. (42) and (43), the best-fit orbit parameters of the S2 star are provided in Ref. [23]—e.g., $a = 125.058 \pm 0.041$ mas, $e = 0.884649 \pm 0.000066$, and so on. This suggests that our preliminary bound on the value of $s\Omega$ is negative, and the negative value corresponds to the scale-dependent Planck stars. According to Eq. (42), the preliminary bounds on Ω or $\tilde{\omega}$ for scale-dependent Planck stars and renormalization group improved Schwarzschild black holes are shown in Table I. We give the preliminary bound on the scale-dependent Planck stars, for the first time, by using the result of the GRAVITY observations for the S2 star. For the renormalization group improved Schwarzschild black holes, the previous work [45] gives the rough and tentative bound on γ and λ based on the measured diameter for M87*'s shadow [11], which is $\gamma \in [0.2, 10]$ and $\lambda_{+} \in [0.02, 0.22]$ (indicated as λ in Ref. [45]). When $\gamma \in [0.2, 10]$, our preliminary bound on λ_{+} gives the range from 0.004 to 0.04 (see Fig. 3), which is tighter than the previous result [45] constrained by the shadow size.

TABLE I. Bounds on the scale-dependent Planck stars (SDPSs) and the renormalization group improved Schwarzschild black holes (RGIBHs) using the results from the periastron advance and the shadow size.

Observation	GRAVITY	EHT
$s\Omega$	$(-0.53 \pm 1.01) \times 10^3$	$-0.09 \lesssim s\Omega \lesssim 1.53$
$s \tilde{\omega} $	$(-0.80 \pm 1.53) \times 10^{92}$	$-1.36 \times 10^{88} \lesssim s \tilde{\omega} \lesssim 2.32 \times 10^{89}$

Since $\Omega \equiv |\tilde{\omega}|/m^2 > 0$, we can reduce the ranges of Ω further for two spacetimes with the results of GRAVITY. The range of Ω for $s = -1$ becomes $(0, 1.54 \times 10^3)$, while the range for $s = 1$ turns into $(0, 0.48 \times 10^3)$. The allowed ranges of $\Omega(\gamma, \lambda_{\mp})$ have been depicted in Fig. 3. In the figure, light blue shaded regions are the allowed ones for γ and λ_{\mp} , and the white regions are excluded for the parameters γ and λ_{\mp} based on our preliminary bound. This indicates that the variation range of γ increases slowly with the growth of λ_{-} ; see the blue shaded region of the left panel in Fig. 3. For the renormalization group improved Schwarzschild black holes, however, the range for $\Omega \in (0, 0.48 \times 10^3)$ is too large to be represented by the right panel in Fig. 3. In the theoretical point of view, from Eq. (8), it is found that $\Omega_{+} \rightarrow 1$ when $\gamma \rightarrow 0$, and $\Omega_{+} \rightarrow 0$ when $\gamma \rightarrow \infty$. It turns out that $\Omega = \lambda_{+}\Omega_{+}$ is always between 0 and 1 when the event horizons exist for the black holes. When we consider the smaller allowed range with $\Omega \in (0, 0.04)$, the allowed range of $\Omega(\gamma, \lambda_{+})$ has been plotted in the inset of the right panel in Fig. 3. We can see that the variation range of γ increases sharply with λ_{+} . We also find that there is still a white region for a larger allowed range of $\Omega(\gamma, \lambda_{+})$ with $\Omega > 0.04$.

It is worth emphasizing that, in our estimation and the uncertainty for $s\Omega$ in Eq. (42), we consider the variances of

the variables in Eq. (41). Besides this, although Ref. [23] presents the orbit fit's posterior distribution, we ignore the relevant covariance in these variables because these correlation coefficients cannot be obtained directly. In our work, the bound given in Eq. (42) is derived with the best-fit orbit parameters. The orbital parameters (e.g., a , e , $m_{\text{SgrA*}}$) should be correlated to $s\Omega$, more or less. The modified periastron advance of the S2 star [e.g., Eq. (38)] due to $s\Omega$ may be reabsorbed in our result of $s\Omega$ partially. Given that, our result might overestimate the bound on $s\Omega$ because of the parameters' correlations. For this issue, Ref. [164] gives some more discussion in more detail. Thus, we only give the preliminary bound on $s\Omega$ instead of a genuine constraint on the scale-dependent Planck stars and the renormalization group improved Schwarzschild black holes based on a full statistical analysis by using the whole observational dataset. In our future work, we will consider this issue carefully if the data can be made publicly available. Besides, there exists a strong parameter degeneracy between γ and λ_{\mp} in $s\Omega(\gamma, \lambda_{\mp})$ [e.g., $\Omega = \lambda_{-}\Omega_{-}(\gamma)$ for $s = -1$ and $\Omega = \lambda_{+}\Omega_{+}(\gamma)$ for $s = 1$; see Eqs. (8)–(10)]. In order to constrain the various parameters γ and λ_{\mp} simultaneously, the best that we can do is to combine the other new data with other observations into the GRAVITY data to break the parameter degeneracy in the future.

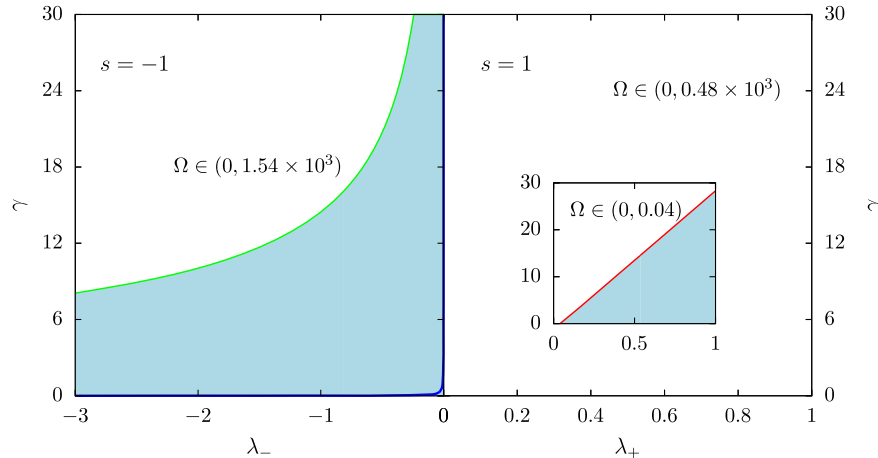


FIG. 3. The allowed ranges of $\Omega(\gamma, \lambda_{\mp})$ with various s under our preliminary bound based on GRAVITY. Here, $s = -1$ denotes the scale-dependent Planck stars (left), where $\Omega(\gamma, \lambda_{-}) \in (0, 1.54 \times 10^3)$ based on Table I, and it depicts different colored regions. The other case represents the renormalization group improved Schwarzschild black holes (right), and the preliminary bound gives $\Omega(\gamma, \lambda_{+}) \in (0, 0.48 \times 10^3)$, which displays the allowed range with a small region based on our preliminary bound. The light blue shaded regions are the allowed ones, while the white regions are excluded based on our preliminary bound (see Table I). The subpanel in the right figure corresponds to the smaller allowed range with $\Omega(\gamma, \lambda_{+}) \in (0, 0.04)$ and shows different colored regions.

B. Photon sphere and shadow

According to Eq. (1), it is shown that the bound on $s|\tilde{\omega}|$ will be improved with EHT observation by up to 3 orders of magnitude, since the experimental system scale L for the EHT is nearly $3R_{\text{Schw}}/2$. Therefore, we will consider the photon sphere and shadow size of the scale-dependent Planck stars and the renormalization group improved Schwarzschild black holes in this subsection.

The radius of the photon sphere x_m is defined as the circular orbit for the lightlike particle based on Eq. (29)—namely, $A(x)_{,x}C(x) - A(x)C(x)_{,x} = 0$. The impact parameter u is given by [165]

$$u = \sqrt{\frac{C(x)}{A(x)}}, \quad (44)$$

and u_m is the shadow size evaluated at x_m . In contrast with the S2's periastron advance, the photon sphere and shadow in two spacetimes depend on both parameters: $s|\tilde{\omega}|$ and γ . Supposing that $\gamma \simeq s\Omega$ in the metric (5), we deduce

$$-0.09 \lesssim s\Omega \lesssim 1.53 \quad (45)$$

or

$$-1.36 \times 10^{88} \lesssim s|\tilde{\omega}| \lesssim 2.32 \times 10^{89}, \quad (46)$$

based on the shadow results of Sgr A* from VLTI [17–22]. In comparison to the bound from the periastron advance [Eqs. (42) and (43)], the bound on $s|\tilde{\omega}|$ from EHT observation is improved by up to 3 or 4 orders of magnitude; see Table I. Even so, it also makes the bound many orders of magnitude larger.

IV. PERIODIC ORBITS

In the strong gravitational field, one specific subclass of bound orbits for the timelike particle are periodic or quasiperiodic ones, which possess the rational or irrational number q [see Eq. (30)] [127]. In this section, we will seek the periodic or quasiperiodic motions for timelike particles around two spacetimes. An attempt is made to distinguish the scale-dependent Planck stars from the renormalization group improved Schwarzschild black holes by the periodic orbits in the strong gravitational field.

The bound orbits of a timelike particle usually lie between the innermost stable circular orbit (ISCO) and the marginally bound orbit. In Sec. II, when taking the circular orbital characteristics of two spacetimes into account, the innermost stable circular orbit has been studied for the cases with the event horizon(s) [Eq. (26)] and horizonless [Eq. (27)] by the radial motion $R(x)$ [Eq. (16)]. As the name indicates, the ISCO is the last stable circular orbit for a particle revolving around the Planck stars or the black holes [161]. The marginally bound orbit, on the other

hand, is defined as a unstable circular orbit whose energy is equal to the rest mass of the particle [161]. Therefore, the marginally bound orbit satisfies $E^2 = 1$ and $R(x)_{,x} = 0$. It is important to note that small perturbations can cause a particle moving in the marginally bound orbit to ultimately escape from the gravity of the Planck stars or black holes. When the timelike particle is located between the innermost stable circular orbit and the marginally bound orbit, the radial motion $R(x)$ can be used to analyze the relevant bound orbital characteristics.

When $\gamma = 10$, Fig. 4 demonstrates the variation of $R(x)$ with different values λ_{\mp} for $l = (l_{\text{ISCO}} + l_{\text{MBO}})/2$ and various values of E (shown by different colors). Here, l_{ISCO} and l_{MBO} represent the angular momentums of the innermost stable circular orbit and the marginally bound orbit for the particle, respectively. ‘‘Schw’’ denotes the Schwarzschild case. There exist three extremal points in the panel labeled (d2) at bottom right due to the horizonless situation for the renormalization group improved Schwarzschild black holes, while the other cases in Fig. 4 admit two extremal points. A value for the energy E that is either too small too big makes the curves of $R(x)$ only a root, which can never have bound orbits. The bound orbits around the Planck stars and the holes can be allowable only if the radial motion $R(x)$ at least has two roots with opposite signs. For example, the light purple curves in Fig. 4 panels labeled (a1)–(d1) and (a2)–(c2) have two roots, and the intersection parts of the light purple curves with $R(x) = 0$ permit such bound orbits. For panel (d2) of Fig. 4, however, the light purple curves have three roots, and the parts between the last two roots can allow bound orbits. As a result, for one given energy E , the turning points can be derived by solving $R(x) = 0$. According to the above characteristics, one can plot the (l, E) allowed regions corresponding to the timelike particle's bound orbits, as shown in Fig. 5.

The left column in Fig. 5 depicts the (l, E) allowed region of the bound orbits for a timelike particle around scale-dependent Planck stars ($s = -1$) with different values of γ and λ_- , while the right column in Fig. 5 shows the orbits around renormalization group improved Schwarzschild black holes ($s = 1$). The lower and upper curves in each shaded region stand for the lower and upper bounds, respectively. This suggests that, for the scale-dependent Planck stars, the (l, E) allowed regions of the bound orbits are extremely sensitive to the parameter γ , and their energies and angular momenta increase with the increase of γ . Besides this, the parameter λ_- has an visible impact on the change of the (l, E) allowed region. It also shows that the shaded area for the (l, E) allowed region decreases as λ_- when the parameter γ is fixed. For renormalization group improved Schwarzschild black holes, the parameters γ and λ_+ have a smaller effect on the (l, E) allowed region of the bound orbits in comparison to the case for the Planck stars. The above properties can equip us to seek possible

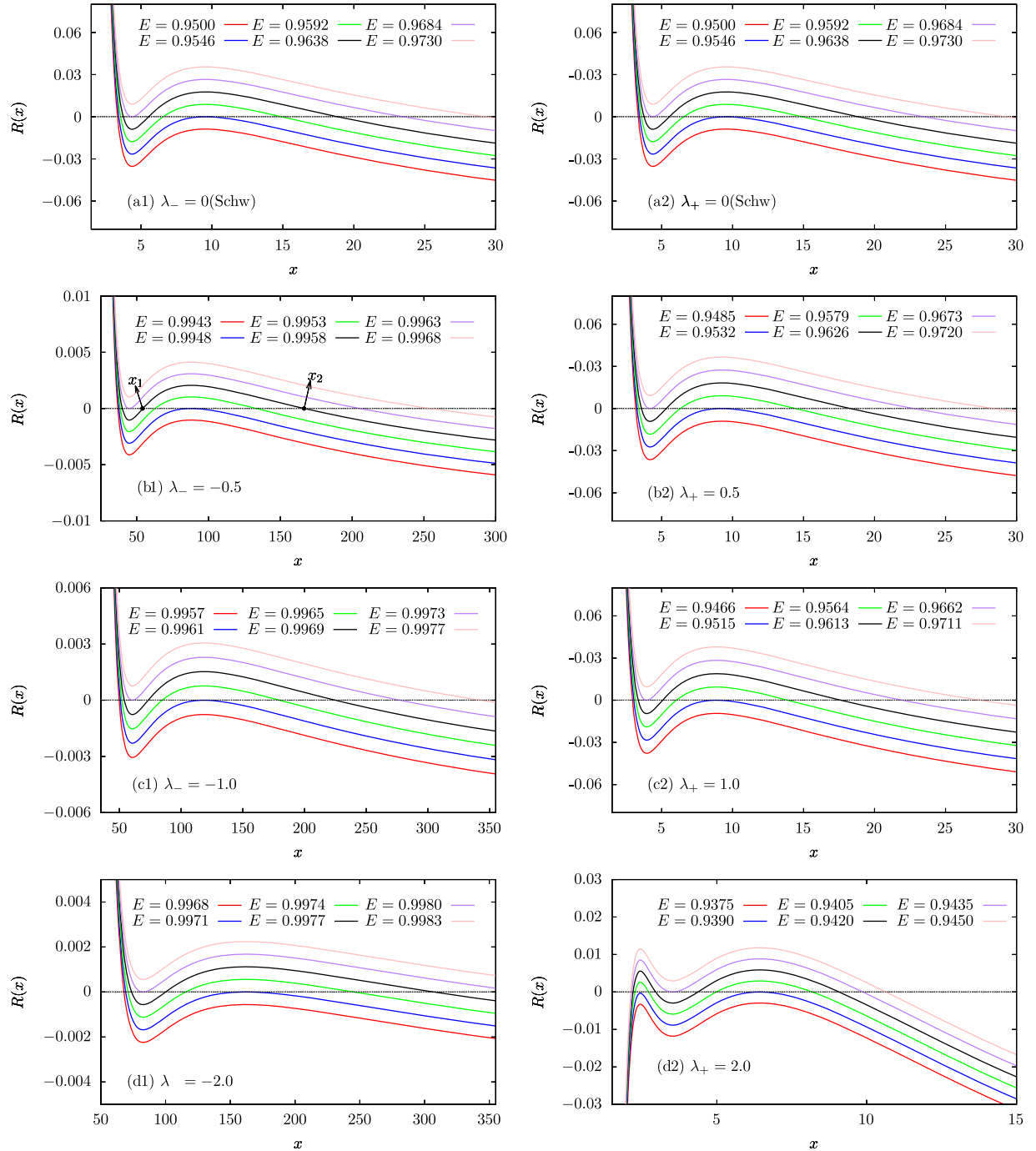


FIG. 4. The radial motion $R(x)$ varies with x for a timelike particle around the scale-dependent Planck stars [$s = -1$ for panels labeled (a1),(b1),(c1), and (d1)] and the renormalization group improved Schwarzschild black holes [$s = 1$ for panels labeled (a2),(b2),(c2), and (d2)] with various values λ_{\mp} and E when $\gamma = 10$ and $l = (l_{\text{ISCO}} + l_{\text{MBO}})/2$. Note that “Schw” denotes the Schwarzschild case.

differences between the periodic orbits around scale-dependent Planck stars and those around renormalization group improved Schwarzschild black holes.

In a strong gravitational field, the periodic or quasiperiodic orbits can be described by q , which can be specified by

three integers (z, w, v) as $q = w + v/z$. The integers z and w are the zoom number and the whirl number, while the integer v represents the vertex number (see Ref. [127] for details). Based on Eqs. (30), (31), and (34), it can be seen that q depends on the angular momentum l , the energy E ,

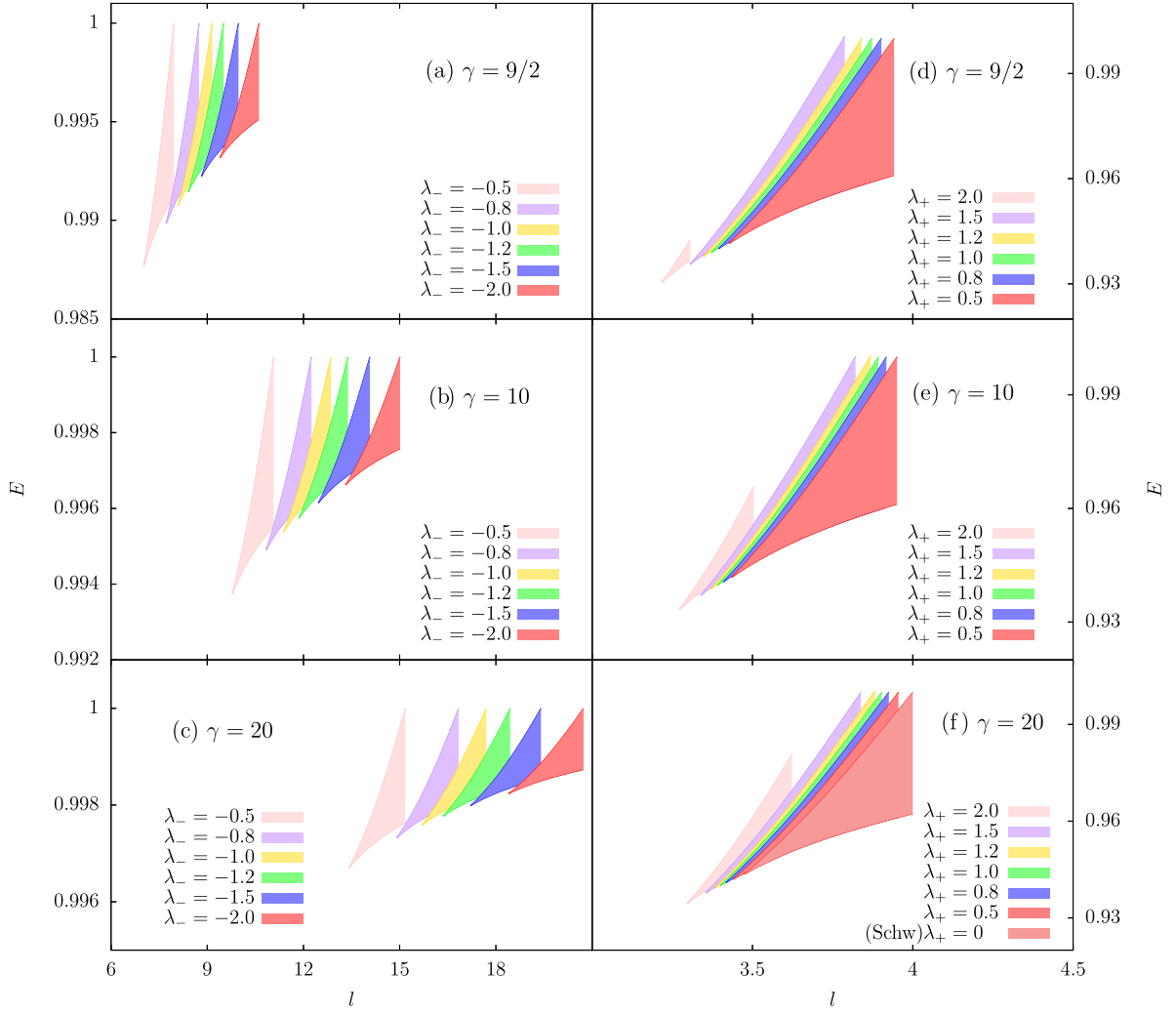


FIG. 5. The (l, E) allowed regions of a timelike particle’s bound orbits around scale-dependent Planck stars [$s = -1$ for panels labeled (a)–(c)] and renormalization group improved Schwarzschild black holes [$s = 1$ for panels labeled (d)–(f)] with different values of γ and λ_{\mp} .

and the metric functions (17) and (18). This means that given the same values of E and l , two different sets of (γ, λ_{\mp}) can generate very different periodic orbits represented by q . Similar behavior in the periastron advance in the weak gravitational field was also discussed in Sec. III A.

When the various (l, E) regions in Fig. 5 overlap with different values of (γ, λ_{\mp}) , the bound orbits for the (quasi) periodic orbits can be present when E and l take the same values; see Fig. 5. Otherwise, with given values of (γ, λ_{\mp}) , we cannot simultaneously plot bound orbits with the same values of E and l under a nonoverlapping areas for the (l, E) allowed regions in Fig. 5. In order to reveal the characteristics for the periodic orbits for two spacetimes, we plot Fig. 6 with a fixed γ . The first and second rows in Fig. 6 show the periodic and quasiperiodic orbits of a timelike particle around scale-dependent Planck stars, and the third and fourth rows give its orbits around renormalization group improved Schwarzschild black holes. The orbits in each row share the same l and E . For instance, all

orbits have $E = 0.993841$ and $l = 8.8$ in the first row of Fig. 6. The particle’s orbit around scale-dependent Planck stars gives a perfect periodic orbit with $\lambda_- = -1.2$ and has only one zoom number. Although the orbit for $\lambda_- = -1.0$ also has a periodic orbit in the same row, its zoom number is changed to 3. As the value of λ_- increases further (to, say, -0.8) the zoom number becomes nearly 5. Conversely, a slight decrease in λ_- can make the particle’s orbit into a nonbound one (denoted as “N.A.”). Also, in the third row of Fig. 6 shared with $E = 0.963354$ and $l = 3.6$, there exists a nonbound orbit for the Schwarzschild case ($\lambda_+ = 0$). However, the (quasi)periodic orbits appear in the renormalization group improved Schwarzschild black holes with the same values of l and E . With the slight increase of λ_+ , the zoom-whirl behaviors change from $q \approx 2 + 4/5$ to $q \approx 3 + 1/2$, and even to $q = 1 + 2/3$.

With a fixed γ , Fig. 6 demonstrates that small variations of λ_{\mp} might not only make bound orbits change from quasiperiodic to periodic ones, but also cause them to jump

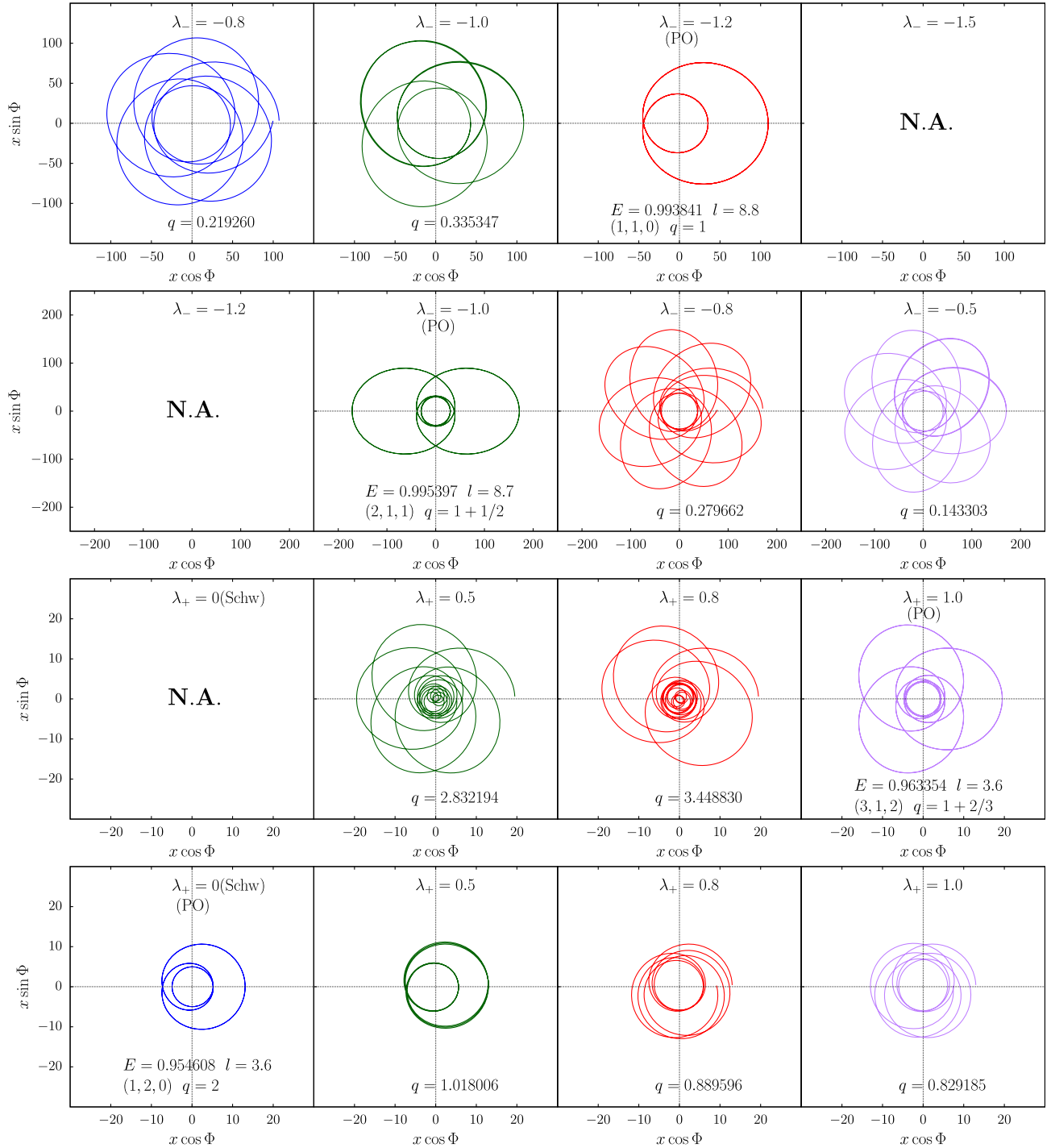


FIG. 6. The periodic orbits (denoted by "PO") and quasiperiodic orbits of a timelike particle around scale-dependent Planck stars and renormalization group improved Schwarzschild black holes with the same values of l and E on each row, for two different sets of λ_{\mp} when $\gamma = 9/2$. Cases of nonbound orbits are marked by "N.A.".

to nonbound orbits. In particular, the orbits for scale-dependent Planck stars and for renormalization group improved Schwarzschild black holes present quite distinguishable behaviors. Different values of λ_{\mp} can cause particles to change from a periodic orbit to a quasiperiodic one even out of the bound orbits. This may provide the

possibility to distinguish between the scale-dependent Planck stars and the renormalization group improved Schwarzschild black holes using information from the (quasi)periodic orbits in the strong gravitational field. The future of radio astronomy with the Square Kilometre Array (SKA) [166], with the observations of a

few radio stars in the central region of our Galaxy, may provide an opportunity to test two spacetimes with unprecedented astrometric accuracy and angular resolution. This will be a huge challenge due to the high density and strong turbulence of the plasma in the central region of the Galaxy, which can strongly affect the light propagation in a curved spacetime.

Based on Refs. [129–131], on the other hand, the gravitational waves emitted from periodic orbits around (non)classical black holes can be used for probing alternative theories of gravity in the strong gravitational field. This motivates us to investigate a preliminary study of the gravitational waveforms generated by the periodic orbits of a small body around scale-dependent Planck stars or renormalization group improved Schwarzschild black holes, such as an extreme mass ratio inspiral system. This kind of binary system will be one of the main targets of some spaceborne gravitational wave detectors in the future—e.g., LISA [167], Taiji [168], and Tianqin [169]. With the same method as Refs. [129–131], we derive the corresponding periodic orbit by treating the small body as a timelike particle. Then, considering “kludge” gravitational waveforms developed in Ref. [170], one can obtain the corresponding gravitational waves by using the equation

$$h_{ij} = \frac{4G\eta M}{c^4 D_L} \left(v_i v_j - \frac{m}{r} n_i n_j \right), \quad (47)$$

up to the quadratic order [129–131] by adopting the adiabatic approximation. In Eq. (47), m and M are the masses of the small body and the supermassive one, respectively. $\eta = Mm/(M+m)^2$. D_L is the luminosity distance. v_i is the spatial velocity of the small body around the scale-dependent Planck star or the renormalization group improved Schwarzschild black hole. Finally, n_i is the direction of the separation vector between the small body and the Planck star or the black hole.

In order to construct two tension polarizations, the gravitational wave can be projected onto a detector-adapted coordinate system [171], where the coordinate directions are given by

$$e_x = (\cos \zeta, \sin \zeta, 0), \quad (48)$$

$$e_y = (\cos \iota \sin \zeta, \cos \iota \cos \zeta, -\sin \iota), \quad (49)$$

$$e_z = (\sin \iota \sin \zeta, \sin \iota \cos \zeta, \cos \iota), \quad (50)$$

where ζ is the longitude of the periastron and ι is the inclination angle. These two angles can be set to any value—e.g., $\pi/4$. Based on the above basis, the transverse traceless tensor polarizations, h_+ and h_\times , are written as [171]

$$h_+ = -\frac{2\eta}{D_L} \frac{G^2 M^2}{c^4 r} (1 + \cos^2 \iota) \cos(2\phi + 2\zeta), \quad (51)$$

$$h_\times = -\frac{4\eta}{D_L} \frac{G^2 M^2}{c^4 r} \cos \iota \sin(2\phi + 2\zeta). \quad (52)$$

In panels (a_1) and (a_2) of Fig. 7, as an example, we plot the gravitational waveforms generated by the periodic orbits around scale-dependent Planck stars and renormalization group improved Schwarzschild black holes with $(z, w, v) = (3, 1, 2)$. Here, the masses of the small body and the supermassive one are $m = 10M_\odot$ and $M = 10^7 M_\odot$, respectively, and $D_L = 200$ Mpc.

In panels (b_1) and (b_2) of Fig. 7, the transverse-traceless tensor polarizations are displayed with respect to the proper time τ (s). The purple, green, and red curves correspond to $(\gamma = 9/2, \lambda_- = -1.0)$, $(\gamma = 10, \lambda_- = -0.5)$, and $(\gamma = 10, \lambda_- = -1.0)$, respectively. In panels (b_3) and (b_4), h_+ and h_\times are also shown with respect to τ (s), where the purple and green curves correspond to $(\gamma = 10, \lambda_+ = 1.0)$ and $(\gamma = 9/2, \lambda_+ = 1.0)$, and the red curve represents the Schwarzschild case ($\lambda_+ = 0$). The plus h_+ and the cross h_\times clearly show the zoom-whirl behaviors of the corresponding periodic orbits. The number of quiet phases of gravitational waves is the same as the number of leaves in the periodic orbit, while the number of louder glitches between the phases is the same as the number of whirls in the periodic orbits. In particular, changes in γ and λ_\mp cause a shift in the phase and amplitude of the gravitational waveform. The increase of γ and the decrease of λ_- result in an increase in the time τ for one orbital period, and in a reduction in amplitude. These properties suggest that the gravitational wave signals radiated by the periodic orbit can also help us to distinguish the scale-dependent Planck stars from the renormalization group improved Schwarzschild black holes.

In the present work, by adopting the adiabatic approximation, we neglect the influence of gravitational radiation on one periodic orbit. This kind of neglect is justified, since the timescale for the orbit’s decay due to gravitational wave emission [172] is

$$\tau_{\text{GW}} \sim \frac{c^5 a^4}{96G^3 m M (M+m) f(e)}, \quad (53)$$

$$f(e) = (1 - e^2)^{-7/2} \left(1 + \frac{73}{24} e^2 + \frac{37}{96} e^4 \right) \quad (54)$$

in the extreme mass ratio inspiral system. If we take the small body’s orbital period T to be periodic, then the small body on an eccentric $e = 0.8$, $T = 0.1$ yr orbit around the supermassive body based on Eq. (53) has

$$\frac{\tau_{\text{GW}}}{T} \sim 10^8 \gg 1. \quad (55)$$

Then, the influence of gravitational radiation on the periodic orbits can be neglected during one whole orbital

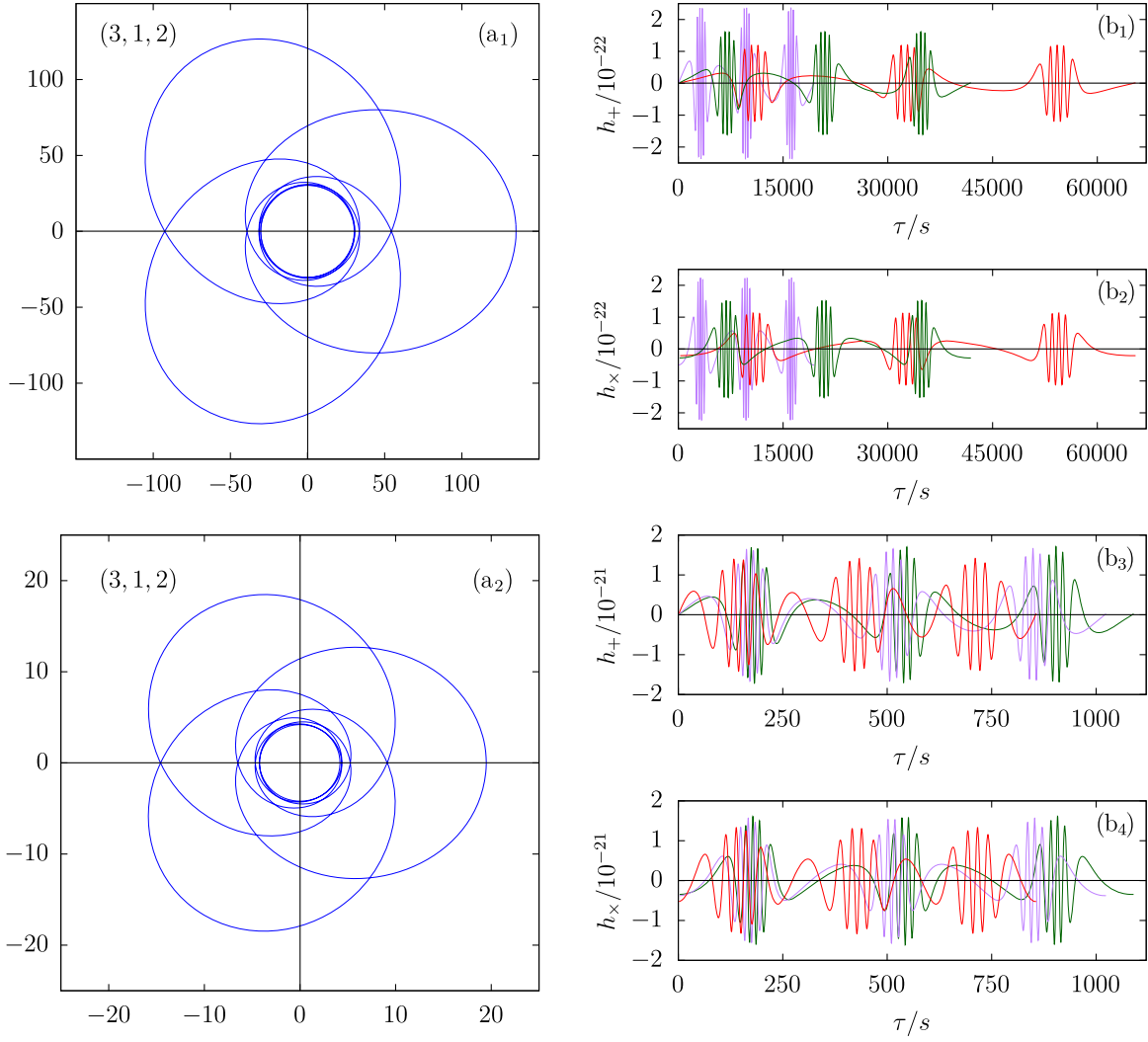


FIG. 7. Panels (a₁) and (a₂) show the periodic orbits around scale-dependent Planck stars and renormalization group improved Schwarzschild black holes with the zoom-whirl behavior of $(z, w, v) = (3, 1, 2)$ ($q = 1 + 2/3$). In panels (b₁) and (b₂), the transverse-traceless tensor polarizations are displayed with respect to the proper time τ (s). The purple, green, and red curves correspond to $(\gamma = 9/2, \lambda_- = -1.0)$, $(\gamma = 10, \lambda_- = -0.5)$, and $(\gamma = 10, \lambda_- = -1.0)$, respectively. In panels (b₃) and (b₄), h_+ and $h_×$ are also shown with respect to τ (s). The purple and green curves correspond to $(\gamma = 10, \lambda_+ = 1.0)$ and $(\gamma = 9/2, \lambda_+ = 1.0)$. The red curve represents the Schwarzschild case ($\lambda_+ = 0$).

period. Even for one small semimajor axis ($a = 50R_{\text{Schw}}$) and more eccentric orbits ($e = 0.9$), it can be approximated as stationary—e.g., $\tau_{\text{GW}}/T \sim 10^5$. Although the effect of gravitational radiation on the periodic orbits are not important for a single periodic orbit, such effects for observations over longer periods of time will need to be considered. We will leave the detailed research on this issue to future work.

V. CONCLUSIONS AND DISCUSSION

In this paper, we mainly focus on the difference between a test timelike particle's motions around scale-dependent Planck stars ($s = -1$) and its motions around renormalization group improved Schwarzschild black holes ($s = +1$).

We first concentrate on their circular orbital characteristics, and we find the existence of stable and unstable circular orbits and the dependence of the innermost stable circular orbit on the parameters γ and λ_{\mp} . This shows that, in comparison to black holes, the parameter γ have more influence on the stable and unstable circular orbits for scale-dependent Planck stars. Subsequently, by deriving a particle's relativistic periastron advance for two spacetimes in the weak gravitational field, a preliminary bound on the scale-dependent Planck stars and the renormalization group improved Schwarzschild black holes is estimated by using the precession of the S2 star around Sgr A* detected by GRAVITY. The bound we obtain in this work is $s|\tilde{\omega}| = (-0.80 \pm 1.53) \times 10^{92}$. With consideration of the shadow result from EHT, the bound is improved by up to

3 or 4 orders of magnitude: $-1.36 \times 10^{88} \lesssim s|\tilde{\omega}| \lesssim 2.32 \times 10^{89}$. This indicates that the existence of Planck stars may be possible due to a negative value of $s|\tilde{\omega}|$. Furthermore, by using the particle's radial equation of motion, the allowed regions (l, E) for the bound orbits under two models are taken into account. It is found that the allowed regions (l, E) are strongly dependent on the parameter γ for the scale-dependent Planck stars, while the contrary is the case for the renormalization group improved Schwarzschild black holes. We also exhibit a particle's periodic orbits around Planck stars and black holes. It is found that small variations in λ_{\mp} make the particle's orbits alternate back and forth from periodic to quasiperiodic orbits, or even jump to a nonbound orbit in two spacetimes. We discuss briefly the gravitational waveforms radiated from one single periodic motion for a small body which orbits a scale-dependent Planck star or the renormalization group improved Schwarzschild black hole by adopting the adiabatic approximation. Our results reveal that the existence of Planck stars affects both the phases of gravitational waves and their amplitudes, while the existence of black holes mainly affects the waves' phases. These results may provide a valuable clue for distinguishing scale-dependent Planck stars from renormalization group improved Schwarzschild black holes by using the motions of a test timelike particle.

Our approaches in the present work are phenomenological. By comparing with the effective field theory, the value of the theoretical prediction for the strength of coupling $s|\tilde{\omega}|$ is nearly order 1. However, our bound on $s|\tilde{\omega}|$ according to existing observations is many orders of magnitude larger than the theoretical prediction due to the large size of L and the huge mass of m_{\bullet} . Even now, there exist some observations for stellar-mass black holes, where the bound on $s|\tilde{\omega}|$ will be up to $\sim 10^{79}$, and it is still a large one. In order to give the tightest bound on $s|\tilde{\omega}|$ in the strong gravitational field, corresponding experiments would have to be conducted at scales much larger than the Planck length. This kind of experiment has not yet been done. As we know, it is not easy to greatly improve the experiment's precision. In order to detect such quantum-corrected effects experimentally in the near future, if a small black hole is

observed, we can give a tighter bound on $s|\tilde{\omega}|$. For this reason, a primordial black hole or even a mini-black hole would be a beneficial observation target, because these tiny black holes' masses might be much less than the mass of the Sun. It also makes their shadow size much smaller.

On the other hand, the two spacetimes we considered here are all nonspinning, whereas astrophysical black holes will nearly always have some spin. Although this kind of nonspinning limit might be suitable for bound orbits adequately far from the black hole/Planck star, or even for very slowly spinning cases, one still needs to consider the spin for those much closer to its center, resulting in more novel and challenging properties. In addition, the bound on $s\Omega$ in this paper is obtained by using the least-squares method, which gives the roughest and the most preliminary estimation of the parameter $s\Omega$. A more complete statistical analysis would be a genuine constraint on scale-dependent Planck stars and renormalization group improved Schwarzschild black holes based on a full statistical analysis with the whole observational dataset. It should be emphasized that the only GRAVITY data (even if the data can be made publicly available) cannot break the parameter $\Omega(\gamma, \lambda_{\mp})$ degeneracy. We look forward to the ultraprecise and ultrasensitive astrometry to be conducted by the future observations (including the Square Kilometre Array [166] and the next-generation Very Large Array [173], etc.). Although the effects of gravitational radiation on the periodic orbits are not important for a single orbital period, such effects for observations over longer periods of time will need to be considered. These issues we mention will be our future prospects.

ACKNOWLEDGMENTS

The work of X.-M. D. is funded by the Natural Science Foundation of China under Grants No. 12173094, No. 11773080, and No. 11473072. The work of L. H. is supported by the National Natural Science Foundation of China under Grants No. 12173094 and No. 12163003. The authors appreciate the support from the Purple Mountain Observatory.

-
- [1] C. M. Will, *Theory and Experiment in Gravitational Physics* (Cambridge University Press, Cambridge, England, 1993).
 - [2] C. M. Will, *Living Rev. Relativity* **17**, 4 (2014).
 - [3] L. Iorio, *Mon. Not. R. Astron. Soc.* **518**, 2599 (2023).
 - [4] Y. Xie and X.-M. Deng, *Mon. Not. R. Astron. Soc.* **438**, 1832 (2014).
 - [5] LIGO Scientific and Virgo Collaborations, *Phys. Rev. Lett.* **116**, 061102 (2016).
 - [6] LIGO Scientific and Virgo Collaborations, *Phys. Rev. X* **6**, 041015 (2016).
 - [7] LIGO Scientific and Virgo Collaborations, *Phys. Rev. Lett.* **116**, 241103 (2016).
 - [8] LIGO Scientific and Virgo Collaborations, *Phys. Rev. Lett.* **118**, 221101 (2017).
 - [9] LIGO Scientific and Virgo Collaborations, *Astrophys. J. Lett.* **851**, L35 (2017).

- [10] LIGO Scientific and Virgo Collaborations, *Phys. Rev. Lett.* **119**, 141101 (2017).
- [11] Event Horizon Telescope Collaboration, *Astrophys. J. Lett.* **875**, L1 (2019).
- [12] Event Horizon Telescope Collaboration, *Astrophys. J. Lett.* **875**, L2 (2019).
- [13] Event Horizon Telescope Collaboration, *Astrophys. J. Lett.* **875**, L3 (2019).
- [14] Event Horizon Telescope Collaboration, *Astrophys. J. Lett.* **875**, L4 (2019).
- [15] Event Horizon Telescope Collaboration, *Astrophys. J. Lett.* **875**, L5 (2019).
- [16] Event Horizon Telescope Collaboration, *Astrophys. J. Lett.* **875**, L6 (2019).
- [17] Event Horizon Telescope Collaboration, *Astrophys. J. Lett.* **930**, L12 (2022).
- [18] K. Akiyama *et al.* (Event Horizon Telescope Collaboration), *Astrophys. J. Lett.* **930**, L13 (2022).
- [19] K. Akiyama *et al.* (Event Horizon Telescope Collaboration), *Astrophys. J. Lett.* **930**, L14 (2022).
- [20] Event Horizon Telescope Collaboration, *Astrophys. J. Lett.* **930**, L15 (2022).
- [21] Event Horizon Telescope Collaboration, *Astrophys. J. Lett.* **930**, L16 (2022).
- [22] Event Horizon Telescope Collaboration, *Astrophys. J. Lett.* **930**, L17 (2022).
- [23] Gravity Collaboration, *Astron. Astrophys.* **636**, L5 (2020).
- [24] Y. Du, S. Tahura, D. Vaman, and K. Yagi, *Phys. Rev. D* **103**, 044031 (2021).
- [25] A. Zulianello, R. Carballo-Rubio, S. Liberati, and S. Ansoldi, *Phys. Rev. D* **103**, 064071 (2021).
- [26] R. Carballo-Rubio, F. Di Filippo, S. Liberati, C. Pacilio, and M. Visser, *J. High Energy Phys.* **05** (2021) 132.
- [27] J. Mazza, E. Franzin, and S. Liberati, *J. Cosmol. Astropart. Phys.* **04** (2021) 082.
- [28] O. Y. Tsupko, *Phys. Rev. D* **89**, 084075 (2014).
- [29] P. Jai-akson, A. Chatrabhuti, O. Evnin, and L. Lehner, *Phys. Rev. D* **96**, 044031 (2017).
- [30] X. Lu and Y. Xie, *Eur. Phys. J. C* **81**, 627 (2021).
- [31] Y.-X. Gao and Y. Xie, *Eur. Phys. J. C* **82**, 162 (2022).
- [32] R. Carballo-Rubio, F. Di Filippo, and S. Liberati, *arXiv*: 2106.01530.
- [33] P. I. Jefremov, O. Y. Tsupko, and G. S. Bisnovaty-Kogan, *Phys. Rev. D* **91**, 124030 (2015).
- [34] M. Favata, *Phys. Rev. D* **84**, 124013 (2011).
- [35] R. C. Nunes, S. Pan, and E. N. Saridakis, *Phys. Rev. D* **98**, 104055 (2018).
- [36] J. Levi Said, J. Mifsud, J. Sultana, and K. Zarb Adami, *J. Cosmol. Astropart. Phys.* **06** (2021) 015.
- [37] J. Levi Said, J. Mifsud, D. Parkinson, E. N. Saridakis, J. Sultana, and K. Zarb Adami, *J. Cosmol. Astropart. Phys.* **11** (2020) 047.
- [38] P. G. S. Fernandes, P. Carrilho, T. Clifton, and D. J. Mulryne, *Phys. Rev. D* **104**, 044029 (2021).
- [39] P. G. S. Fernandes, P. Carrilho, T. Clifton, and D. J. Mulryne, *Classical Quantum Gravity* **39**, 063001 (2022).
- [40] L. Mei and L. Huang, *Eur. Phys. J. C* **84**, 76 (2024).
- [41] X. Lu and Y. Xie, *Eur. Phys. J. C* **80**, 625 (2020).
- [42] C. Liu, T. Zhu, Q. Wu, K. Jusufi, M. Jamil, M. Azreg-Aïnou, and A. Wang, *Phys. Rev. D* **101**, 084001 (2020).
- [43] K. Jusufi, M. Jamil, H. Chakrabarty, Q. Wu, C. Bambi, and A. Wang, *Phys. Rev. D* **101**, 044035 (2020).
- [44] G. Abbas, A. Mahmood, and M. Zubair, *Phys. Dark Universe* **31**, 100750 (2021).
- [45] X. Lu and Y. Xie, *Eur. Phys. J. C* **79**, 1016 (2019).
- [46] T.-Y. Zhou, W.-G. Cao, and Y. Xie, *Phys. Rev. D* **93**, 064065 (2016).
- [47] F.-Y. Liu, Y.-F. Mai, W.-Y. Wu, and Y. Xie, *Phys. Lett. B* **795**, 475 (2019).
- [48] X.-Y. Zhu and Y. Xie, *Eur. Phys. J. C* **80**, 444 (2020).
- [49] L. Jenks, K. Yagi, and S. Alexander, *Phys. Rev. D* **102**, 084022 (2020).
- [50] Y.-X. Gao and Y. Xie, *Phys. Rev. D* **103**, 043008 (2021).
- [51] X.-T. Cheng and Y. Xie, *Phys. Rev. D* **103**, 064040 (2021).
- [52] X. Lu, F.-W. Yang, and Y. Xie, *Eur. Phys. J. C* **76**, 357 (2016).
- [53] X. Wu, Y. Wang, W. Sun, F.-Y. Liu, and W.-B. Han, *Astrophys. J.* **940**, 166 (2022).
- [54] X. Wu and H. Zhang, *Astrophys. J.* **652**, 1466 (2006).
- [55] X. Wu and Y. Xie, *Phys. Rev. D* **76**, 124004 (2007).
- [56] S. Dalui, B. R. Majhi, and P. Mishra, *Phys. Lett. B* **788**, 486 (2019).
- [57] X. Wu and Y. Xie, *Phys. Rev. D* **77**, 103012 (2008).
- [58] X. Wu, Y. Wang, W. Sun, and F. Liu, *Astrophys. J.* **914**, 63 (2021).
- [59] Y. Wang, W. Sun, F. Liu, and X. Wu, *Astrophys. J. Suppl. Ser.* **254**, 8 (2021).
- [60] Y. Wang, W. Sun, F. Liu, and X. Wu, *Astrophys. J.* **909**, 22 (2021).
- [61] A.-R. Hu and G.-Q. Huang, *Eur. Phys. J. Plus* **136**, 1210 (2021).
- [62] Y. Wang, W. Sun, F. Liu, and X. Wu, *Astrophys. J.* **907**, 66 (2021).
- [63] D. Yang, W. Cao, N. Zhou, H. Zhang, W. Liu, and X. Wu, *Universe* **8**, 320 (2022).
- [64] H. Zhang, N. Zhou, W. Liu, and X. Wu, *Gen. Relativ. Gravit.* **54**, 110 (2022).
- [65] R. N. Izmailov, R. K. Karimov, A. A. Potapov, and K. K. Nandi, *Ann. Phys. (Amsterdam)* **413**, 168069 (2020).
- [66] G. Y. Tuleganova, R. N. Izmailov, R. K. Karimov, A. A. Potapov, and K. K. Nandi, *Gen. Relativ. Gravit.* **52**, 31 (2020).
- [67] M. Caruana, G. Farrugia, and J. Levi Said, *Eur. Phys. J. C* **80**, 640 (2020).
- [68] G. A. R. Franco, C. Escamilla-Rivera, and J. Levi Said, *Eur. Phys. J. C* **80**, 677 (2020).
- [69] A. Bonanno and M. Reuter, *Phys. Rev. D* **62**, 043008 (2000).
- [70] G. Lambiase and F. Scardigli, *Phys. Rev. D* **105**, 124054 (2022).
- [71] F. Scardigli and G. Lambiase, *Phys. Rev. D* **107**, 104001 (2023).
- [72] J. F. Donoghue, *Phys. Rev. Lett.* **72**, 2996 (1994).
- [73] J. F. Donoghue, *Phys. Rev. D* **50**, 3874 (1994).
- [74] H. W. Hamber and S. Liu, *Phys. Lett. B* **357**, 51 (1995).
- [75] N. E. Bjerrum-Bohr, J. F. Donoghue, and B. R. Holstein, *Phys. Rev. D* **67**, 084033 (2003).
- [76] N. E. J. Bjerrum-Bohr, J. F. Donoghue, and B. R. Holstein, *Phys. Rev. D* **71**, 069903 (2005).
- [77] N. E. Bjerrum-Bohr, J. F. Donoghue, and B. R. Holstein, *Phys. Rev. D* **68**, 084005 (2003).

- [78] P. Bargeño, S. Bravo Medina, M. Nowakowski, and D. Batic, *Europhys. Lett.* **117**, 60006 (2017).
- [79] R. Yang, *Phys. Rev. D* **92**, 084011 (2015).
- [80] A. Bonanno and M. Reuter, *Int. J. Mod. Phys. D* **13**, 107 (2004).
- [81] J. Rayimbaev, A. Abdujabbarov, M. Jamil, B. Ahmedov, and W.-B. Han, *Phys. Rev. D* **102**, 084016 (2020).
- [82] C. Rovelli and F. Vidotto, *Int. J. Mod. Phys. D* **23**, 1442026 (2014).
- [83] R. M. Wald, *Phys. Rev. D* **10**, 1680 (1974).
- [84] V. P. Frolov and A. A. Shoom, *Phys. Rev. D* **82**, 084034 (2010).
- [85] V. P. Frolov and P. Krtouš, *Phys. Rev. D* **83**, 024016 (2011).
- [86] V. P. Frolov, *Phys. Rev. D* **85**, 024020 (2012).
- [87] J. Kovář, O. Kopáček, V. Karas, and Z. Stuchlík, *Classical Quantum Gravity* **27**, 135006 (2010).
- [88] J. Kovář, P. Slaný, C. Cremaschini, Z. Stuchlík, V. Karas, and A. Trova, *Phys. Rev. D* **90**, 044029 (2014).
- [89] A. Abdujabbarov and B. Ahmedov, *Phys. Rev. D* **81**, 044022 (2010).
- [90] S. Shaymatov, B. Narzilloev, A. Abdujabbarov, and C. Bambi, *Phys. Rev. D* **103**, 124066 (2021).
- [91] C. Bambi, *arXiv:2106.04084*.
- [92] S. Liberati, C. Pfeifer, and J. J. Relancio, *arXiv:2106.01385*.
- [93] E. Franzin, S. Liberati, J. Mazza, A. Simpson, and M. Visser, *J. Cosmol. Astropart. Phys.* **07** (2021) 036.
- [94] A. A. Abdujabbarov, B. J. Ahmedov, and N. B. Jurayeva, *Phys. Rev. D* **87**, 064042 (2013).
- [95] B. Narzilloev, J. Rayimbaev, A. Abdujabbarov, B. Ahmedov, and C. Bambi, *Eur. Phys. J. C* **81**, 269 (2021).
- [96] B. Narzilloev, J. Rayimbaev, S. Shaymatov, A. Abdujabbarov, B. Ahmedov, and C. Bambi, *Phys. Rev. D* **102**, 044013 (2020).
- [97] J. Vrba, A. Abdujabbarov, A. Tursunov, B. Ahmedov, and Z. Stuchlík, *Eur. Phys. J. C* **79**, 778 (2019).
- [98] B. Narzilloev, A. Abdujabbarov, C. Bambi, and B. Ahmedov, *Phys. Rev. D* **99**, 104009 (2019).
- [99] B. Narzilloev, J. Rayimbaev, S. Shaymatov, A. Abdujabbarov, B. Ahmedov, and C. Bambi, *Phys. Rev. D* **102**, 104062 (2020).
- [100] L. Iorio and F. Zhang, *Astrophys. J.* **839**, 3 (2017).
- [101] S. Hussain, I. Hussain, and M. Jamil, *Eur. Phys. J. C* **74**, 3210 (2014).
- [102] S. Chakrabarti and J. L. Said, *Phys. Rev. D* **101**, 124044 (2020).
- [103] G. F. Rubilar and A. Eckart, *Astron. Astrophys.* **374**, 95 (2001).
- [104] R. Javlon, D. Alexandra, U. Camci, A. Abdujabbarov, and B. Ahmedov, *arXiv:2010.04969*.
- [105] J.-T. Yao and X. Li, *Phys. Rev. D* **108**, 084067 (2023).
- [106] K. Isomura, R. Suzuki, and S. Tomizawa, *Phys. Rev. D* **107**, 084003 (2023).
- [107] L. Iorio and E. N. Saridakis, *Mon. Not. R. Astron. Soc.* **427**, 1555 (2012).
- [108] L. Iorio, *J. Cosmol. Astropart. Phys.* **07** (2012) 001.
- [109] Y. Xie and X.-M. Deng, *Mon. Not. R. Astron. Soc.* **433**, 3584 (2013).
- [110] L. Iorio, *Mon. Not. R. Astron. Soc.* **437**, 3482 (2014).
- [111] M. L. Ruggiero and N. Radicella, *Phys. Rev. D* **91**, 104014 (2015).
- [112] I. De Martino, R. Lazkoz, and M. De Laurentis, *Phys. Rev. D* **97**, 104067 (2018).
- [113] X.-M. Deng and Y. Xie, *Eur. Phys. J. C* **75**, 539 (2015).
- [114] T. Damour and G. Esposito-Farèse, *Phys. Rev. D* **53**, 5541 (1996).
- [115] M. Kramer, I. H. Stairs, R. N. Manchester, M. A. McLaughlin, A. G. Lyne, R. D. Ferdman, M. Burgay, D. R. Lorimer, A. Possenti, N. D'Amico, J. M. Sarkissian, G. B. Hobbs, J. E. Reynolds, P. C. C. Freire, and F. Camilo, *Science* **314**, 97 (2006).
- [116] M. De Laurentis, R. De Rosa, F. Garufi, and L. Milano, *Mon. Not. R. Astron. Soc.* **424**, 2371 (2012).
- [117] M. De Laurentis and I. De Martino, *Mon. Not. R. Astron. Soc.* **431**, 741 (2013).
- [118] X.-M. Deng, Y. Xie, and T.-Y. Huang, *Phys. Rev. D* **79**, 044014 (2009).
- [119] X.-M. Deng, *Eur. Phys. J. Plus* **132**, 85 (2017).
- [120] L. Iorio, *Mon. Not. R. Astron. Soc.* **411**, 167 (2011).
- [121] M. Vargas dos Santos and D. F. Mota, *Phys. Lett. B* **769**, 485 (2017).
- [122] M. L. Ruggiero and L. Iorio, *J. Cosmol. Astropart. Phys.* **06** (2020) 042.
- [123] K. Glampedakis and D. Kennefick, *Phys. Rev. D* **66**, 044002 (2002).
- [124] L. Barack and C. Cutler, *Phys. Rev. D* **69**, 082005 (2004).
- [125] R. Haas, *Phys. Rev. D* **75**, 124011 (2007).
- [126] J. Healy, J. Levin, and D. Shoemaker, *Phys. Rev. Lett.* **103**, 131101 (2009).
- [127] J. Levin and G. Perez-Giz, *Phys. Rev. D* **77**, 103005 (2008).
- [128] R. Grossman, J. Levin, and G. Perez-Giz, *Phys. Rev. D* **88**, 023002 (2013).
- [129] A. Maselli, N. Franchini, L. Gualtieri, T. P. Sotiriou, S. Barsanti, and P. Pani, *New Astron.* **6**, 464 (2022).
- [130] D. Liang, R. Xu, Z.-F. Mai, and L. Shao, *Phys. Rev. D* **107**, 044053 (2023).
- [131] Z.-Y. Tu, T. Zhu, and A. Wang, *Phys. Rev. D* **108**, 024035 (2023).
- [132] V. Misra and J. Levin, *Phys. Rev. D* **82**, 083001 (2010).
- [133] G. Z. Babar, A. Z. Babar, and Y.-K. Lim, *Phys. Rev. D* **96**, 084052 (2017).
- [134] S.-W. Wei, J. Yang, and Y.-X. Liu, *Phys. Rev. D* **99**, 104016 (2019).
- [135] D. Pugliese, H. Quevedo, and R. Ruffini, *Eur. Phys. J. C* **77**, 206 (2017).
- [136] P. Bambhaniya, A. B. Joshi, D. Dey, and P. S. Joshi, *Phys. Rev. D* **100**, 124020 (2019).
- [137] P. Bambhaniya, D. Dey, A. B. Joshi, P. S. Joshi, D. N. Solanki, and A. Mehta, *Phys. Rev. D* **103**, 084005 (2021).
- [138] D. N. Solanki, P. Bambhaniya, D. Dey, P. S. Joshi, and K. N. Pathak, *Eur. Phys. J. C* **82**, 77 (2022).
- [139] C.-Q. Liu, C.-K. Ding, and J.-L. Jing, *Commun. Theor. Phys.* **71**, 1461 (2019).
- [140] T.-Y. Zhou and Y. Xie, *Eur. Phys. J. C* **80**, 1070 (2020).
- [141] R. Wang, F. Gao, and H. Chen, *Ann. Phys. (Amsterdam)* **447**, 169167 (2022).
- [142] J. Zhang and Y. Xie, *Eur. Phys. J. C* **82**, 854 (2022).
- [143] J. Zhang and Y. Xie, *Eur. Phys. J. C* **82**, 471 (2022).

- [144] J. Zhang and Y. Xie, *Astrophys. Space Sci.* **367**, 17 (2022).
- [145] Á. Duenas-Vidal and J. Segovia, *Phys. Rev. D* **108**, 086006 (2023).
- [146] M.-H. Wu, H. Guo, and X.-M. Kuang, *Phys. Rev. D* **107**, 064033 (2023).
- [147] B. Gao and X.-M. Deng, *Ann. Phys. (Amsterdam)* **418**, 168194 (2020).
- [148] X.-M. Deng, *Eur. Phys. J. C* **80**, 489 (2020).
- [149] X.-M. Deng, *Phys. Dark Universe* **30**, 100629 (2020).
- [150] B. Gao and X.-M. Deng, *Eur. Phys. J. C* **81**, 983 (2021).
- [151] H.-Y. Lin and X.-M. Deng, *Phys. Dark Universe* **31**, 100745 (2021).
- [152] B. Gao and X.-M. Deng, *Mod. Phys. Lett. A* **36**, 2150237 (2021).
- [153] H.-Y. Lin and X.-M. Deng, *Eur. Phys. J. Plus* **137**, 176 (2022).
- [154] H.-Y. Lin and X.-M. Deng, *Universe* **8**, 278 (2022).
- [155] H.-Y. Lin and X.-M. Deng, *Eur. Phys. J. C* **83**, 311 (2023).
- [156] J. Levin and R. Grossman, *Phys. Rev. D* **79**, 043016 (2009).
- [157] R. Grossman and J. Levin, *Phys. Rev. D* **79**, 043017 (2009).
- [158] Y.-K. Lim and Z. C. Yeo, *Phys. Rev. D* **109**, 024037 (2024).
- [159] W. Rindler, *Relativity: Special, General, and Cosmological*, 2nd ed. (Oxford University Press, Oxford, UK, 2006).
- [160] S. Chandrasekhar, *The Mathematical Theory of Black Holes* (Oxford University Press, New York, 1998).
- [161] R. M. Wald, *General Relativity* (University of Chicago Press, Chicago, 1984).
- [162] A. Tucker and C. M. Will, *Classical Quantum Gravity* **36**, 115001 (2019).
- [163] S. A. Klioner and S. M. Kopeikin, *Astrophys. J.* **427**, 951 (1994).
- [164] L. Bernus, O. Minazzoli, A. Fienga, M. Gastineau, J. Laskar, and P. Deram, *Phys. Rev. Lett.* **123**, 161103 (2019).
- [165] K. S. Virbhadra and G. F. R. Ellis, *Phys. Rev. D* **62**, 084003 (2000).
- [166] R. Braun, T. Bourke, J. A. Green, E. Keane, and J. Wagg, in *Advancing Astrophysics with the Square Kilometre Array (AASKA14)* (SKA Organisation, Chesire, 2015), p. 174.
- [167] LISA Collaboration, [arXiv:1702.00786](https://arxiv.org/abs/1702.00786).
- [168] B.-R. Wang and J. Li, [arXiv:2311.07116](https://arxiv.org/abs/2311.07116).
- [169] J. Luo, L.-S. Chen, H.-Z. Duan, Y.-G. Gong, S. Hu, J. Ji, Q. Liu, J. Mei, V. Milyukov, M. Sazhin, C.-G. Shao, V. T. Toth, H.-B. Tu, Y. Wang, Y. Wang, H.-C. Yeh, M.-S. Zhan, Y. Zhang, V. Zharov, and Z.-B. Zhou, *Classical Quantum Gravity* **33**, 035010 (2016).
- [170] S. Babak, H. Fang, J. R. Gair, K. Glampedakis, and S. A. Hughes, *Phys. Rev. D* **75**, 024005 (2007).
- [171] E. Poisson and C. M. Will, *Gravity: Newtonian, Post-Newtonian, Relativistic* (Cambridge University Press, Cambridge, England, 2014).
- [172] C. W. Misner, K. S. Thorne, and J. A. Wheeler, *Gravitation* (Freeman, San Francisco, 1973).
- [173] E. J. Murphy *et al.*, *Science with a Next Generation Very Large Array*, Astronomical Society of the Pacific Conference Series Vol. 517, edited by E. Murphy (2018), p. 3, [arXiv:1810.07524](https://arxiv.org/abs/1810.07524).